AN EFFICIENT AND COMPUTATIONALLY ATTRACTIVE LOCALIZATION ALGORITHM UNDER LARGE EQUAL RADIUS SCENARIO

A Thesis presented to

the Faculty of the Graduate School

at the University of Missouri

In Partial Fulfillment

of the Requirements for the Degree

Master of Science

---

by

SASA LI

Dr. Dominic Ho, Thesis Supervisor

MAY 2015

The undersigned, appointed by the Dean of the Graduate School, have examined the thesis entitled:

AN EFFICIENT AND COMPUTATIONALLY ATTRACTIVE LOCALIZATION ALGORITHM UNDER LARGE EQUAL RADIUS SCENARIO

presented by Sasa Li,

a candidate for the degree of Master of Science and hereby certify that, in their opinion, it is worthy of acceptance.

Dr. Dominic Ho

Dr. Satish Nair

Dr. Yi Shang

ACKNOWLEDGMENTS

I would like to express my special appreciation and thanks to my advisor Professor Dr. Dominic Ho, you have been a tremendous mentor for me. I would like to thank you for encouraging my research and for allowing me to grow as a research scientist. Your advice on both research as well as on my career have been priceless. I would also like to thank my committee members, professor Satish Nair, professor Yi Shang for serving as my committee members. I also want to thank you for letting my defense be an enjoyable moment, and for your brilliant comments and suggestions, thanks to you.

Special thanks to my family. Words cannot express how grateful I am to my parents for all of the sacrifices that you've made on my behalf. Without your support, I would not have gotten nearly this far and I cannot thank you enough! I also would like to express appreciation to my boyfriend Eric Roberts who always strands behind me and encourages me to strive towards my goal.

TABLE OF CONTENTS

LIST OF TABLES

LIST OF FIGURES

ABSTRACT

We give a review of the basic techniques and positioning methods in the field of source localization. The linear least squares (LLS) is widely used due to the computational efficiency. We introduce the Large Equal Radius (LER) scenario based on satellite geolocation problem. Two algorithms based on LLS, SCWLS and DMVLS, solving the localization problems under LER scenario, are presented, but they involve time-consuming computations and/or complex root selection strategy. The two-step weighted least squares by Chan and Ho is a common LLS method, but its performance degrades significantly under the Large Equal Radius (LER) conditions. Here we propose a computationally friendly and efficient estimator based on TDOA measurements under LER scenario. The performance of the proposed estimator is analyzed, and it's shown theoretically that the position covariance matrices can approach the Cramér-Rao Lower Bound (CRLB) when the LER conditions are sufficiently satisfied. Simulation results are included and assessed by comparing with the performance of SCWLS and DMVLS, as well as the CRLB. We also analyze the performance degradation due to the presence of sensor position error, and take them into account in the proposed estimator. The proposed estimator can eventually improve the source location estimate accuracy and reach the CRLB when sensor position errors are small. Theoretical development are provided and simulations are included to evaluate its localization accuracy by comparing with algorithms ignoring sensor position errors as well as CRLB.

Chapter 1

Introduction

1.1 Background

Accurate source localization has gained much research interest in recent years, motivated by the rapidly increasing demand for services and systems that depends on accurate location estimations. A wide variety of applications have been developed based on source localization in areas like sonar [1] [2], radar [3], global positioning system (GPS) [4] [5], wireless sensor networks [6] [7], emergency response [8] and human-computer interactions [9] [10].

Sonar and radar systems can not only detect targets but also localize them through bearing and range estimation. Depending on different situations, these objectives of bearing and range estimation can be accomplished actively or passively [11]. In passive sonar systems, the target is detected from acoustic signals emitted by the target, by receiving signals at spatially separated points, passive sonar can locate the target

from the range estimate using time delays. This system provides bearing and range information on a target by comparing its received signal at a multiplicity of widely separated points along the length of its own ship or along a towed array. The target's bearing is determined by measuring the time difference of the received signals at two difference locations. The time delay can be obtained by cross correlating the received signals from these two points and measuring the displacement of the correlogram peak, then be converted to the range difference [12]. In an active system, a pulse is transmitted to the target and the echo is received. The range of a target is determined using the time delay between the transmission of the pulse and the reception of its echo. Similarly the time delay can be obtained from the cross correlation of the transmitted signal and the received signal.

The Global Positioning System (GPS) is a space-based satellite navigation system that is based on a man-made constellation of 27 Earth-orbiting satellites. GPS can be effectively used for many navigation applications. A GPS receiver placed on the earth can localize its position and get time information in all weather conditions, where there is an unobstructed line of sight (LOS) to four or more GPS satellites. When the LOS is not satisfied, it is not capable of positioning due to signal attenuation at places such as inside building and mines. Scattering environment like the downtown urban areas can also degrade its positioning performance.

Recent years, the advanced technologies in wireless communication and microsystem integration have enabled to develop small, inexpensive and low power consuming sensor nodes that are capable of performing some processing, gathering sensory information and communicating with other connected nodes in the sensor network [13]. These wireless sensor networks (WSNs) have a wide range of applications across many

areas, from medical and clinical research, structural health monitoring, to mission-critical industrial and military applications. For most of the wireless sensor network applications, sensor nodes are placed arbitrarily and their positions need to be known to operate and manage the sensor network. However GPS have not fitted into WSNs well owing to their price, power consumption, accuracy and limitations in their operating system. Therefore, sensor nodes positioning is a critical issue and has become a very active research area.

With the development of mobile technologies, Location Based Services (LBS) promisingly improve people's daily life. Such services include mobile gaming, mobile advertisement, predicted content pre-fetching and push, warning for traffic jams and etc., which all need an accurate position of the user [14]. Furthermore, since the Federal Communications Commission (FCC) in the United States has adopted rules to improve the 911 services by mandating the accuracy of locating an emergency caller to be within a specified range, even for a wireless phone user [15], accurate and timely position estimates have become more important given the safety issues. In home intelligent robot applications, source localization is also a core technique in conjunction with human-robot interaction that can naturally interact between human and robots . In [10], by using multiple microphones, when the robot's name is called, the speech source is located by the time delay between each two microphones.

In the future, the existing positioning systems used in numerous applications will likely be expanded, in response to new demands. For example, in a self-driving car system, the information on the road condition and traffic may be obtained using various existing positioning systems such as GPS and radar.

1.2 Typical Measurements

The primary function of source localization is to locate a source with respect to a set of sensors (receivers) with known positions. The time of arrival (TOA), time difference of arrival (TDOA), angle of arrival (AOA), and received signal strength (RSS) of the signal emitter are the common measurements used for source localization from static sensors. TOAs, TDOAs, and RSSs are ranged-based measurements and provide the distance information between the signal emitter and sensor receivers, while AOAs are the source bearings relative to the receivers. However, these measurements have non-linear relationships with the source location, and to solve the nonlinear problems and find a closed-form solution is not a trivial task for source localization. In the following summary, we consider a two dimensional space with the true source located at $\mathbf{u}^o = [x^o,\ y^o]^T$ and M receivers located at $\mathbf{s}_i = [x_i,\ y_i]^T,\ i = 1, 2, \cdots, M$.

A comparison summary for the four typical measurement models is provided in Table 1 [13].

1.2.1 Time of Arrival (TOA)

One primary method for determining position location is with TOA measurements. Time of arrival (TOA) is the propagation time from a signal emitter to a remote signal receiver. Since electronmagneic waves propagate at the consistent speed of light ($c = 3 \times 10^8$m/s), the distance from the source to the receivers are proportional to the propagation time. When there is no measurement noises, if a signal from the source takes time t_i to the ith sensor, then the source lies at the range r_i, where

$$r_i = ct_i = \sqrt{(x_i - x^o)^2 + (y_i - y^o)^2}. \tag{1.1}$$

Table 1: Comparison of different measurement models

Model	Location Information	Advantage	Disadvantage
TOA	Range	Accuracy is high.	Time synchronization across source and all receivers is needed. LOS is assumed.
TDOA	Range difference	Accuracy is high. Time synchronization at source is not required.	LOS is assumed.
AOA	Bearing	Only at least two receivers are needed. Time synchronization is not required.	Smart antennas are needed. LOS is assumed.
RSS	Range	Simple and inexpensive. Time synchronization is not required.	Accuracy is low.

Therefore, as shown in Figure 1, each time of arrival corresponds to a circle where the receiver lies in the center and the source is somewhere on the circumference. If TOA measurements are made from the second sensor at a different location, then the source location can be narrowed to the intersection positions of two spheres, which implies two possible source solutions, and data from a third receiver is required to refine the results to a single point. In three dimensional space, the source position is determined by the intersection of three spheres using TOA measurements from three receivers [16] [17]. In general, direct TOA has two problems. First, since time of arrival uses the absolute time arrival at a certain receiver TOA requires high-precision clock synchronization across all the receivers. For example, $1\mu s$ timing error can result in a 300m positioning error. Second, the signal transmitted must have a timestamp label for the receivers to discern the distance the signal has traveled [13]. For this reason, TDOA measurements are more practical for commercial positioning

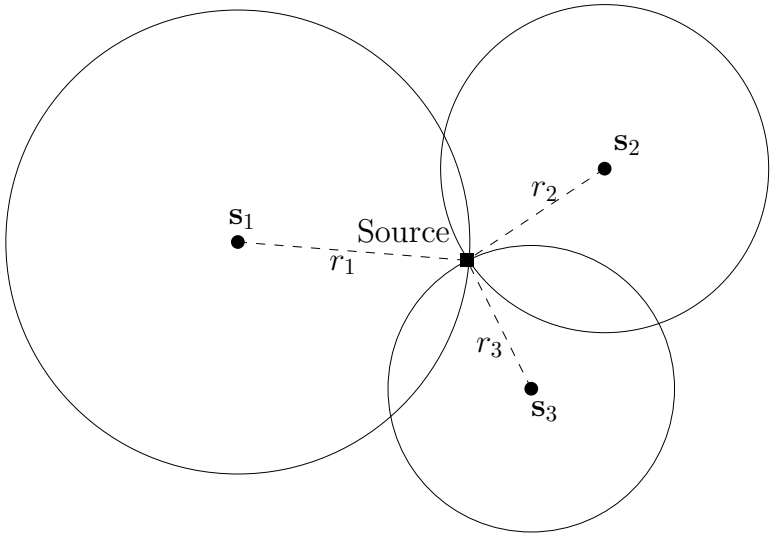

Figure 1: Illustration of source localization using TOAs. $\mathbf{s}_1$,$\mathbf{s}_2$, $\mathbf{s}_3$: receiver locations

systems [18].

1.2.2 Time Difference of Arrival (TDOA)

Instead of using the absolute arrival time, TDOA examines the difference in time at which the signal arrives at multiple receivers. Similar to TOA, by multiplying with the known propagation speed TDOAs indicate the range difference between the source and two receivers. Therefore, each TDOA measurement indicates that the source must lie on the hyperboloid with a consistent range difference between two receivers. Geometrically measuring the difference in distance between two receivers in noise-free conditions results in infinite number of possible source locations and they form a hyperbolic curve. The intersection of at least two hyperbolic curves can help target the source location, as shown in Figure 2. The equation of the hyperboloid is

given by

$$r_{ij} = r_i - r_j = \sqrt{(x_i - x^o)^2 + (y_i - y^o)^2} - \sqrt{(x_j - x^o)^2 + (y_j - y^o)^2}, \qquad (1.2)$$

where $i, j = 1, 2, \cdots, M$ and $i \neq j$.

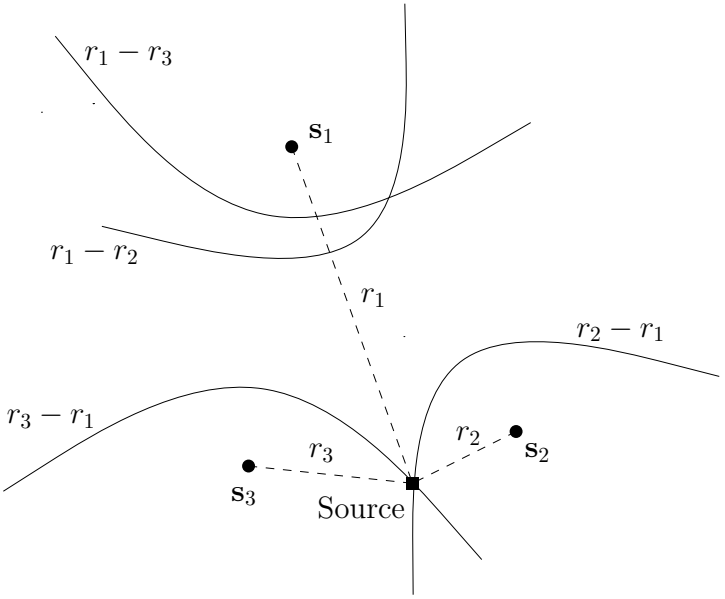

Figure 2: Illustration of source localization using TDOAs. $\mathbf{s}_1$,$\mathbf{s}_2$, $\mathbf{s}_3$: receiver locations

In the absence of measurement noise, a two-dimensional source location can be estimated from the intersection of two or more independently generated hyperboloids, and for a three-dimensional source location, at least three hyperboloids are required to locate the source.

Before evaluating the hyperbolic range equation (1.2), it is important to estimate the range differences r_{ij}, or equivalently the TDOA $t_i - t_j$. Compared to the TOA measurements, TDOA doesn't require a timestamp but also requires the precisely synchronized clock. The generalized cross-correlation method is widely used to obtain these TDOA estimates. Suppose the transmitted signal is $s(t)$, and the signal received

at the ith sensor $x_i = s(t - d_i) + n_i(t)$ is delayed by d_i and corrupted by the noise $n_i(t)$. Similarly, the signal received at the jth sensor $x_j = s(t - d_j) + n_j(t)$ is delayed by d_j and corrupted by the noise $n_j(t)$. The cross-correlation function is given by integrating the lag product of two received signal $x_i,\ x_j$ for a sufficiently long time period T [12],

$$\hat{r}_{i,j}(\tau) = \frac{1}{T} \int_0^T x_i(t) x_j(t - \tau) dt. \tag{1.3}$$

The TDOA estimate is given by the value of τ that maximizes Equation (1.3). The SNR of TDOA estimates can be improved by increasing the integration time period T. Note that we assume the transmitting signal travels in a straight line, which is referred as line-of-sight (LOS) propagation. Otherwise, multipath propagation can cause overlapping cross-correlation peaks and result in significant inaccuracy for TDOA estimates.

1.2.3 Angle of Arrival (AOA)

Angle of arrival (AOA), also called direction of arrival (DOA), has been used widely in sensor networks, radar tracking, and vehicle navigation systems [19] [20] [21] [22]. In general, an angle of arrival estimate is made from a base station using a directional antenna such as a phased array of two or more antenna elements to measure the AOA of the incident signal. As shown in Figure 3, for each AOA, we can draw a line of bearing (LOB) from the source to the receiver, and the intersection of at least two LOBs will give the source location. One current application of AOA is in the geo-location of cell phones. The AOAs of the cell phone's signal from multiple base stations could be combined to determine the phone's location to comply with

regulations that require cell systems to report the location of a cell phone placing an emergency (i.e., 911) call [23].

AOA estimation can achieve higher accuracy than RSS-based localization approaches, since the phase of received signal is more stable than the received signal strength. In addition, while range-based measurement require three or more receivers to target the source location, two antenna arrays can suffice to localize the source position given an effective AOA estimation scheme [24]. However, the array must be carefully calibrated over all measured angles, as well as frequency and temperature, which is an expensive operation, in terms of the cost of both computational storage and periodcally performing the array calibration.

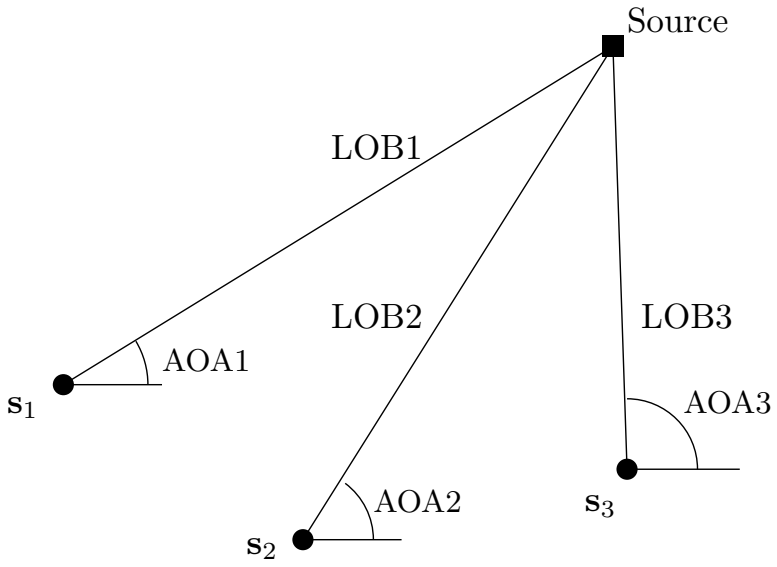

Figure 3: Illustration of source localization using AOAs. $\mathbf{s}_1$,$\mathbf{s}_2$, $\mathbf{s}_3$: receiver locations

1.2.4 Received Signal Strength (RSS)

Besides TOA and TDOA, Received Signal Strength (RSS) is another kind of range-based measurements. This technique has been employed in both cellular [25] and

wireless sensor networks [7] [26] [27]. It is assumed that the signal strength decay over distance follows a distribution that is known as a priori. This distribution is often a function of the transmitted power, path loss constant, and the distance between the source and sensors, which is used for converting one or several signal strength measurements into distance estimates. This positioning scheme is simpler than using TOA and TDOA measurements, because the synchronization among the source and/or sensors are both required by TOA and TDOA measurements, more processing, more communication and thus more energy [28].

The RSS measurement model is formulated as follows. Assuming that the original transmitted power is P_t, and in the absence of disturbance, the average received power at sensor i is denoted by $P_{r,i}$, which is modeled as [22]

$$P_{r,i} = K_i \frac{P_t}{d_i^{\alpha}}, \tag{1.4}$$

where $d_i = \|\mathbf{u}^o - \mathbf{s}_i\|$ is the distance between the source and the ith sensor, α is the path loss constant. In free space $\alpha = 2$, depending on the propagation environment, α can vary from 2 to 5. K_i is the rest of all other factors that will affect the received power at sensor i, including the antenna height and antenna gain.

However RSS-based ranging has several drawbacks, and the distance estimates are inaccurate because of the environment errors, such as the multipath and shadowing effect, and device errors caused by the inter-device differences, depleting batteries and the antenna orientations.

1.3 Large Equal Radius (LER)

There have been numerous algorithms proposed for solving overdetermined systems of the TOA, TDOA or pseudo range geolocation equations, such as Bancroft method [29], Fang method [16], the Taylor expansion method [30], and Chan-Ho method [18]. These techniques have been widely used in various applications such as the Global Positioning System (GPS) and navigations [31]. If the noise is small enough, and the configuration of the satellites is not degenerate, there is little difference among various technique performances [32]. However, a matrix ill-conditioned problem in Chan-Ho method occurs under the Large Equal Radius (LER) conditions. LER has been defined and studied in [33]. Its definition is given by Definition 1:

Definition 1. [33] A satellite-based geolocation problem satisfies the LER conditions for a navigation user (or emitter) on or near the surface of the Earth if all of the satellites are equidistant from the center of the Earth and many Earth radii away.

It is shown in [33] that the usual GPS constellation of satellites where all of the satellites at middle Earth orbit (MEO) distance are sufficiently LER. Here we give a more general definition:

Definition 2. The LER conditions are satisfied if the satellites (or receivers) are equidistant or close to equidistant from some point $\mathbf{P}$ and if the common distance from the satellites (or receivers) to $\mathbf{P}$ is much greater than the distance from the user (or source) to $\mathbf{P}$.

Figure 4 illustrates the LER scenario, compared to the non-LER scenario in Figure 5. Consider M sensors and 1 source. $\mathbf{s}_i$ is the ith sensor location, $i = 1, 2, \cdots, M$, and $\mathbf{u}^o$ is the true source location. Let $R_i = \|\mathbf{s}_i - \mathbf{P}\|$ be the distance from sensor i

to $\mathbf{P}$, R be the common distance from the sensors to $\mathbf{P}$, and $r^o = \|\mathbf{u}^o - \mathbf{P}\|$ be the distance from the source to $\mathbf{P}$. The Definition 2 can be expressed by

$$\begin{aligned} & R_i \approx R, \quad \frac{r^o}{R} \approx 0, \\ & i = 1, 2, \cdots, M. \end{aligned} \tag{1.5}$$

Or equivalently, the LER conditions are satisfied when the distances from the source to all the receivers are identical or approximately the same,

$$r_i^o \approx r_j^o, \ i \neq j, \ i, j = 1, 2, \cdots, M, \tag{1.6}$$

where $r_i^o = \|\mathbf{u}^o - \mathbf{s}_i\|$ denote the distance from the source to the ith sensor.

Suppose $\mathbf{P}$ to be the origin in the coordinate system. We refer the common distance R as the sensor range, and r as the source range. Also we define $\frac{R}{r^o}$ as the sensor range and the source range ratio (hereafter called **range ratio**). The LER conditions are satisfied when the range ratio is large. For some algorithms based on TOA or TDOA measurements, for example, Chan-Ho method [18], their measurement matrices encounter a singularity problem due to the approximately identical or the same measurements, which results in a significant performance degradation. Romero *et al.* [33] analyze and test over a wide range of noise level some of the most popular algorithms for solving overdetermined TOA or pseudo range geolocation equations under LER scenario. They also propose the Dual-root minimum variance least squares (DMVLS). Lin *et al.* [34] also concerns about the positioning performance degradation caused by the ill-conditioned measurement matrix under LER conditions and provide the separated constrained weighted least squares method for optimum estimation

accuracy. Both of their methods will be introduced in Chapter 3.

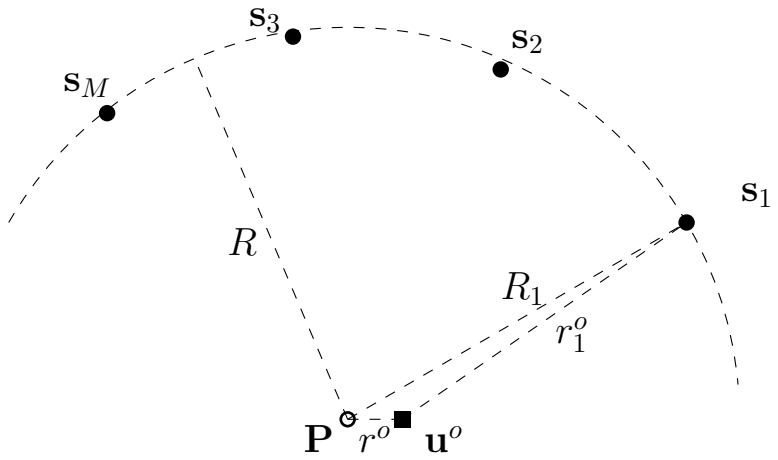

Figure 4: Illustration of the LER localization scenario

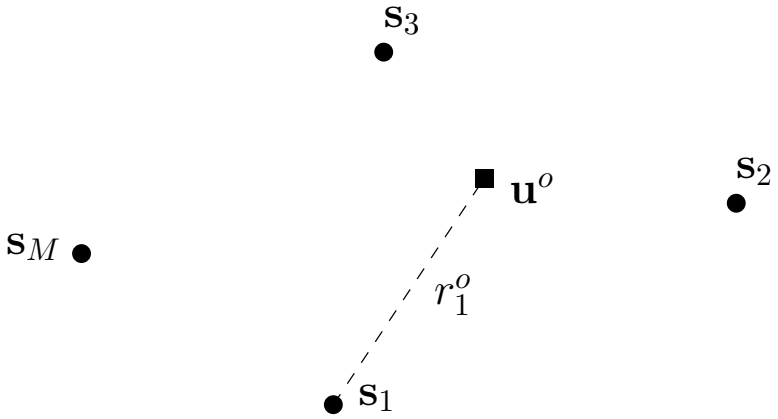

Figure 5: Illustration of the non LER localization scenario

1.4 Sensor Position Errors

Source localization based on TOA/TDOA measurements is an important problem in many applications. The source location estimate accuracy is very sensitive to the sensor position errors and the performance of source localization can be degraded

significantly in the presence of sensor position errors. Using the source location and sensor position setting in Section 3.3.3, Figure 18 shows the difference between the MSE and the theoretical source location estimate accuracy CRLB. For the estimators ignoring sensor position errors, as the sensor position error power increases, the difference is about 3dB to 5dB.

Some papers have analyzed the decrease in performance caused by random sensor position errors, and some studies have been conducted to minimize this degradation [35] [36] [37] [38]. Ho and Ma *et al.* [35] theoretically analyze the degradation in the performance based on TOA source localization. Sensor position errors are included into weighting matrix and they offer a closed-form solution that eventually improves the estimation accuracy in the presence of sensor position errors.

The theoretical analysis of the performance degradation under LER scenario due to sensor position error is presented in Section 3.3.2 and Section 4.3.2 for 2-D and 3-D respectively.

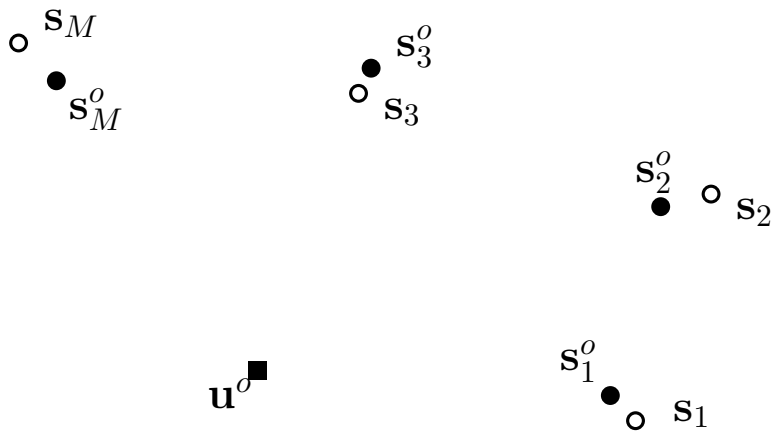

Figure 6: Illustration of the general localization scenario in the presence of sensor position errors. Solid disks denote the unknown true sensor positions, and open circles denote the known erroneous sensor positions

1.5 Motivation and Contribution

LER conditions hold for the usual GPS constellation of satellites where all of the satellites are located at MEO distance. More generally, LER conditions are satisfied when sensors have approximately equal or the same distances to the source, especially when sensors form a uniform circular array (UCA). In practice, the UCA geometry is the optimal configuration for localization [39] when the receivers on the circumference have equal angular spacing and the source is at the center of the circle. Therefore LER scenario often occurs in practical applications, such as a team of unmanned aerial vehicles, maneuver to form an UCA around a source [41], the circular microphone array for speaker localization [42] and sonobuoys deployed in a semi-circular pattern to detect and localize submarines [43].

Chan-Ho method is a classical TDOA-based localization algorithm, however, it will yield exceptionally large localization errors under sufficiently LER scenario. Though studies [33] [34] are available for the source localization under LER scenario, their methods have some obvious drawbacks. Their estimators can reach the optimum performance when TDOA measurement noise is small, but their techniques either include complex polynomial calculations and/or complicated root selection strategy, which consumes more time and energy. We hope to develop an algorithm that not only is computation friendly but also can reach the optimum performance under LER scenario.

In our study, we start with the two dimensional LER scenario and develop a novel localization algorithm by taking advantage of the angles of the sensors with respect to the x-axis. We give a detailed analysis for the CRLB of the true source location as well as the theoretical performance of the proposed method with respect to the mean

square error. It is shown by theory that the proposed method can reach the optimum estimation accuracy CRLB in a wide range of TDOA measurement noise powers. Simulations are performed and the theoretical development is confirmed. Next we expand the proposed method to the three dimensional LER scenario. Similarly, theoretical performance analysis is stated that the proposed method in 3D can reach the optimum performance, which is also confirmed by simulation results. Based on the analysis of the performance degradation caused by sensor position errors, by following the general procedure in [36], we develop a modified estimator that takes into account the sensor position errors and eventually maintain the optimum performance when the sensor position errors are small.

1.6 Conclusion and Content Organization

This chapter has provided an overview of source localization techniques and systems that are currently in use for various applications. These localization systems are usually based on four typical measurements: TOA, TDOA, AOA and RSS. We addressed their basic principles and compared their advantages and disadvantages. We also introduced the concept of LER scenario based on the satellite geolocation and gave a more general definition. In addition, we illustrated the presence of sensor position error in source localization scenario and briefly talked about the estimator performance degradation caused by the sensor position errors. We then explained the motivation for doing the localization algorithm development under LER scenario and pointed out the contributions of our research.

We now give a brief outline of the rest of the thesis.

Chapter 2 first introduces the theoretical optimum source location estimate accuracy, Cramér-Rao Lower Bound (CRLB), for localization problems. Both nonlinear and linear source localization algorithms based on TOA, TDOA, RSS and AOA measurements are presented. Nonlinear algorithms solve the nonlinear equation obtained from the nonlinear relationship between the source location and measurements directly, such as maximum likelihood (ML) estimators. Linear algorithms take advantages of the linearization of the nonlinear equations, like the linear least squares (LLS) and weighted least squares (WLS). Typical LS methods, Chan-Ho method, SCWLS and DMVLS are presented. Then the estimation accuracy for source localization is discussed.

Chapter 3 devises a new source localization algorithm under LER scenario in two-dimensional space. The theoretical CRLB and the mean square error (MSE) analysis is presented. The simulation results are shown to confirm the theoretical developments. The proposed method is also expanded to work in the presence of sensor position error. Its theoretical estimation accuracy is stated and confirmed by the numerical results.

Chapter 4 expands the proposed method from two dimensional space to three dimensional space. Similarly, we provide the theoretical CRLB and the MSE analysis, followed by the simulation results to confirm the theoretical developments. Then the proposed method is expanded to work in the presence of sensor position error, and its theoretical estimation accuracy is stated and confirmed by the numerical results.

Chapter 5 concludes the findings in the research and states the future work.

Chapter 2

Algorithms for Source Localization

In Chapter 2, we introduce the source localization scenario and the theoretical source location estimate accuracy Cramér-Rao Lower Bound (CRLB). We will also present the typical nonlinear and linear approaches, maximum likelihood (ML) estimation and the linear least squares (LLS) method respectively. We then address the two-step LLS method proposed by Chan and Ho, and the other two LLS methods, DMVLS and SCWLS, under LER localization scenario.

2.1 Localization Scenario

We consider one source and M sensors in a source localization scenario. Let $\{*\}^o$ denote the noise-free version of quantity $\{*\}$. The true source location is $\mathbf{u}^o$. The sensor location is denoted by $\mathbf{s}_i,\ i = 1, 2, \cdots, M$. A set of N signal measurement m_i from sensors forms the measurement vector $\mathbf{m} = [m_1, m_2, \cdots, m_N]^T$.

Let $\boldsymbol{\theta}$ be the unknown source location to be estimated. In the absence of ran-

dom measurement noise, m_i is related to the unknown source location $\boldsymbol{\theta}$ through a known nonlinear function $f_i(\boldsymbol{\theta})$ depending on different measurement models. In mathematical form, with measurement noise n_i,

$$m_i = f_i(\boldsymbol{\theta}) + n_i. \tag{2.1}$$

The collection of N equations from (2.1) forms a single measurement vector,

$$\mathbf{m} = \mathbf{f}(\boldsymbol{\theta}) + \mathbf{n}, \tag{2.2}$$

where $\mathbf{f}(\boldsymbol{\theta}) = [f_1(\boldsymbol{\theta}), f_2(\boldsymbol{\theta}), \cdots, f_N(\boldsymbol{\theta})]^T$ and the measurement noise $\mathbf{n} = [n_1, n_2, \cdots, n_N]^T$ is assumed zero-mean Gaussian random vector with an positive-definite covariance matrix $\mathbf{Q}$.

2.2 Estimation Accuracy for Localization

The Cramér-Rao Lower Bound (CRLB) is most often used as a theoretical lower bound for any unbiased estimator, and it can be served as an important benchmark to compare with the mean square error (MSE) of the localization algorithms. Using a Gaussian random signal model, we will derive the CRLB for source location estimate in this scenario. The key in producing the CRLB is to construct the corresponding Fisher information matrix (FIM). The diagonal elements of the FIM increase are the minimum achievable variance values.

Considering a source location vector $\boldsymbol{\theta} = [x, y, z]^T$ in three dimensional space and an unbiased estimator $\hat{\boldsymbol{\theta}}$. Given the general measurement model of Equation 2.2, the

probability density function (pdf) parameterized on $\boldsymbol{\theta}$ is

$$p(\mathbf{m};\boldsymbol{\theta}) = \frac{1}{(2\pi)^{\frac{N}{2}}\det^{\frac{1}{2}}(\mathbf{Q})}\exp\Big[-\frac{1}{2}[\mathbf{m}-\mathbf{f}(\boldsymbol{\theta})]^T\mathbf{Q}^{-1}[\mathbf{m}-\mathbf{f}(\boldsymbol{\theta})]\Big]. \tag{2.3}$$

Taking the logarithm on both sides of (2.3) yields

$$\ln p(\mathbf{m};\boldsymbol{\theta}) = v - \frac{1}{2}[\mathbf{m}-\mathbf{f}(\boldsymbol{\theta})]^T\mathbf{Q}^{-1}[\mathbf{m}-\mathbf{f}(\boldsymbol{\theta})], \tag{2.4}$$

where v is a constant which does not depend on $\boldsymbol{\theta}$.

The standard procedure to compute the CRLB is as follows [44]:

1. Compute the second order derivatives of the logarithm of the measurement PDF with respect to $\boldsymbol{\theta}$, that is $\frac{\partial^2 \ln p(\mathbf{m};\boldsymbol{\theta})}{\partial\boldsymbol{\theta}\partial\boldsymbol{\theta}^T}$.

2. Take expectation of $\frac{\partial^2 \ln p(\mathbf{m};\boldsymbol{\theta})}{\partial\boldsymbol{\theta}\partial\boldsymbol{\theta}^T}$ to yield

$$\mathbf{I}(\boldsymbol{\theta}) = -E\left[\frac{\partial^2 \ln p(\mathbf{m};\boldsymbol{\theta})}{\partial\boldsymbol{\theta}\partial\boldsymbol{\theta}^T}\right], \tag{2.5}$$

   where $\mathbf{I}(\boldsymbol{\theta})$ denotes the FIM.

3. The CRLB for x, y and z are given by the (i,i) element of the inverse of FIM matrix, i.e. $[\mathbf{I}(\boldsymbol{\theta})^{-1}]_{1,1}$, $[\mathbf{I}(\boldsymbol{\theta})^{-1}]_{2,2}$ and $[\mathbf{I}(\boldsymbol{\theta})^{-1}]_{3,3}$ respectively.

The vector parameter CRLB will allow us to place a bound on the variance of each element,

$$var(\hat{\boldsymbol{\theta}}_i) \geq [\mathbf{I}^{-1}(\boldsymbol{\theta})]_{ii}, \tag{2.6}$$

where $\boldsymbol{\theta}_i$ is the ith element in $\boldsymbol{\theta}$.

2.3 Maximum Likelihood Estimation (MLE)

The well known ML estimator is asymptotically efficient. The ML estimator is defined to be the value of $\boldsymbol{\theta}$ that maximizes (2.4). As shown in Figure 7, $\hat{\boldsymbol{\theta}}$ is the solution that maximizes the likelihood function.

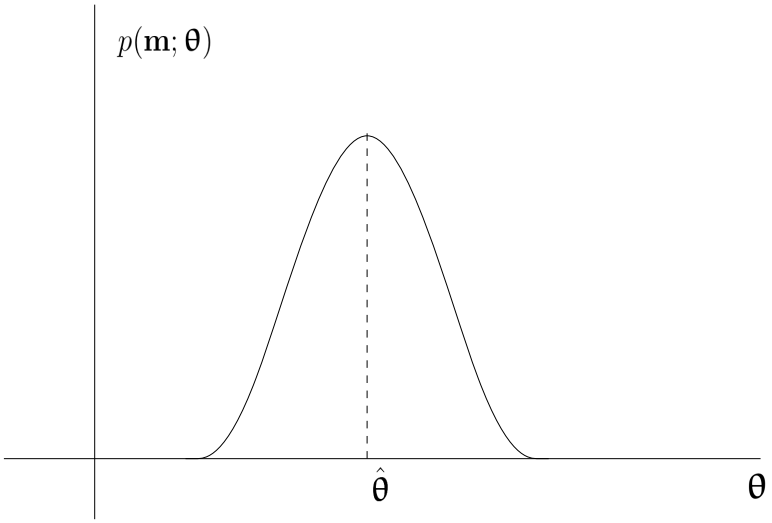

Figure 7: Rationale for maximum likelihood estimator

On the other hand, the MLE of $\boldsymbol{\theta}$ is found by minimizing

$$\mathbf{J}(\boldsymbol{\theta}) = [\mathbf{m} - \mathbf{f}(\boldsymbol{\theta})]^T \mathbf{Q}^{-1} [\mathbf{m} - \mathbf{f}(\boldsymbol{\theta})]. \tag{2.7}$$

When a closed form location expression can not be found for the MLE, a numerical approach employs either a grid search or an iterative maximization of likelihood function [44]. Taylor series is one of the typical iterative procedures and is summarized in this section.

To maximize the log-likelihood function by finding zeros of the derivative function, we assume an initial guess for the source location and approximate by linearizing the

function with respect to this initial guess location. Upon setting the function to zero, we obtain a new guess. By repeating previous procedure until getting some stopping criteria, we can get the final estimate for the source location.

Assuming there is an initial guess $\boldsymbol{\theta}_o$ sufficiently close to the unknown $\boldsymbol{\theta}$, the nonlinear function vector $\mathbf{f}(\boldsymbol{\theta})$ can be linearized through the Taylor series expansion with respect to $\boldsymbol{\theta}_o$,

$$\mathbf{f}(\boldsymbol{\theta}) \simeq \mathbf{f}(\boldsymbol{\theta}_o) + \mathbf{g}(\boldsymbol{\theta}_\mathbf{o})(\boldsymbol{\theta} - \boldsymbol{\theta}_o), \tag{2.8}$$

where

$$\mathbf{g}(\boldsymbol{\theta}_o) = \left.\frac{\partial \ln p(\mathbf{m};\boldsymbol{\theta})}{\partial \boldsymbol{\theta}}\right|_{\boldsymbol{\theta}=\boldsymbol{\theta}_o}. \tag{2.9}$$

Substituting (2.8) into the cost function (2.7), taking derivative and setting it to zero gives the solution

$$\hat{\boldsymbol{\theta}} = \boldsymbol{\theta}_o + [\mathbf{g}(\boldsymbol{\theta}_o)^T \mathbf{Q}^{-1} \mathbf{g}(\boldsymbol{\theta}_o)]^{-1} \mathbf{g}(\boldsymbol{\theta}_o)^T \mathbf{Q}^{-1} [\mathbf{m} - \mathbf{f}(\boldsymbol{\theta}_o)]. \tag{2.10}$$

Next we replace $\boldsymbol{\theta}_o$ in (2.10) by the computed estimate $\hat{\boldsymbol{\theta}}$ and repeat (2.10) until the iteration converges or some stopping criteria is satisfied.

Example 2.1. Consider a 2-D geometry of $M = 4$ sensors with known coordinates at $(5,5)^T$,$(5,-5)^T$,$(-5,5)^T$ and $(-5,-5)^T$, while the unknown source position is $(2,3)^T$. The range difference noise power $c^2\sigma^2$ varies from 10^{-7} to 10^2. Note that the source is located inside the square bounded by the four receivers, but the geometry is not sufficient LER scenario. The start point is initialized as the true source location. 2000 ensemble runs are performed. It's shown in the figure that the Taylor-series method can reach the CRLB at small TDOA measurement noise, and it has a threshold effect when the range difference noise power is equal to 1.

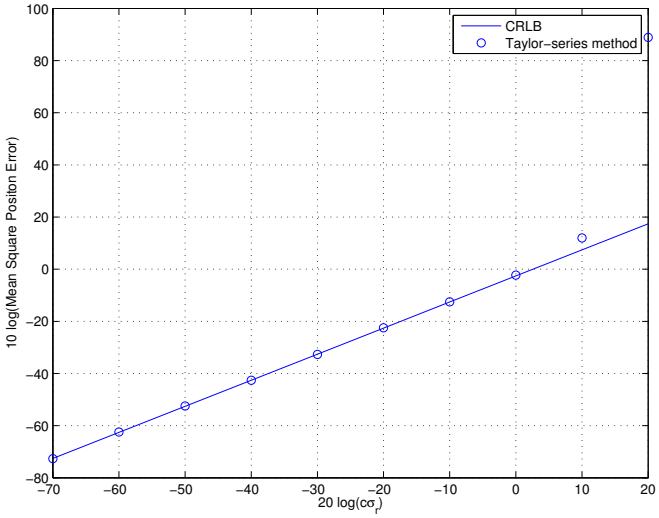

Figure 8: Source localization performance using the Taylor-series method based on TDOA measurements

2.4 Linear Least Squares (LLS)

In the least squares (LS) approach we attempt to minimize the squared difference between the given signal measurements and the assumed or noiseless measurements. To apply the linear least squares (LLS) approach, we assume $\mathbf{f}(\boldsymbol{\theta})$ to be linear in the unknown source location $\boldsymbol{\theta}$,

$$\mathbf{f}(\boldsymbol{\theta}) = \mathbf{G}\boldsymbol{\theta}, \tag{2.11}$$

where the observation matrix $\mathbf{G}$ is a known $N \times p$ matrix ($N > p$) of full rank p. Note that $\mathbf{f}(\boldsymbol{\theta})$ is the noiseless measurement vector whereas $\mathbf{m}$ is the perturbed version. The LS estimator is found by minimizing the cost function

$$\mathbf{J}(\boldsymbol{\theta}) = (\mathbf{m} - \mathbf{G}\boldsymbol{\theta})^T(\mathbf{m} - \mathbf{G}\boldsymbol{\theta}). \tag{2.12}$$

Taking the derivative of $\mathbf{J}(\boldsymbol{\theta})$, we get

$$\frac{\partial \mathbf{J}(\boldsymbol{\theta})}{\partial \boldsymbol{\theta}} = -2\mathbf{G}^T\mathbf{m} + 2\mathbf{G}^T\mathbf{G}\boldsymbol{\theta}. \tag{2.13}$$

Setting the derivative equal to zero yields the LS estimator

$$\hat{\boldsymbol{\theta}} = (\mathbf{G}^T\mathbf{G})^{-1}\mathbf{G}^T\mathbf{m}. \tag{2.14}$$

An extension of the linear LS is to weighted LS. Instead of minimizing (2.12), we include an $N \times N$ positive definite weighting matrix $\mathbf{W} = \mathbf{Q}^{-1}$, so that

$$\mathbf{J}(\boldsymbol{\theta}) = (\mathbf{m} - \mathbf{G}\boldsymbol{\theta})^T\mathbf{W}(\mathbf{m} - \mathbf{G}\boldsymbol{\theta}). \tag{2.15}$$

The general form of the weighted LSE is readily shown to be

$$\hat{\boldsymbol{\theta}} = (\mathbf{G}^T\mathbf{W}\mathbf{G})^{-1}\mathbf{G}^T\mathbf{W}\mathbf{m}, \tag{2.16}$$

and its minimum LS error is

$$\mathbf{J}_{min} = \mathbf{m}^T(\mathbf{W} - \mathbf{W}\mathbf{G}(\mathbf{G}^T\mathbf{W}\mathbf{G}^{-1})\mathbf{G}^T\mathbf{W})\mathbf{m}. \tag{2.17}$$

The LLS technique is widely used in TOA and TDOA based positioning because of it computational efficiency. Chan-Ho method [18] is a popular LLS method based TDOAs that has received a relatively large number of citations. In this section, Chan-Ho method are reviewed and the matrix ill-conditioned problem is noted. Here we also introduce two methods based on LLS that are proposed to solve the ill-conditioned

measurement matrix problem under LER situations as mentioned in section 1.3.

2.4.1 The Method of Chan and Ho

Chan-Ho method is a two-step weighted least squares estimator, which exploits the relationship between the additional variable and the source position [18]. It can provide optimum estimation accuracy equal to Cramér-Rao lower bound (CRLB) at sufficiently small noise conditions. However, when the distances from the source to all receivers are identical or approximately the same, there is an ill-conditioned matrix problem.

Consider a two-dimensional situation with an array of $M \geq 4$ sensors. Let the true source location $\mathbf{u}^o = [x^o,\ y^o]^T$ and the ith sensor location $\mathbf{s}_i = [x_i,\ y_i]^T, i = 1, 2, \cdots, M$. The true distance between the source and the ith sensor,

$$r_i^o = \|\mathbf{u}^o - \mathbf{s}_i\| = \sqrt{(x^o - x_i)^2 + (y^o - y_i)^2},\ i = 1, 2, \cdots, M. \tag{2.18}$$

The true range difference is given by

$$r_{i,1}^o = r_i^o - r_1^o,\ i = 2, 3, \cdots, M. \tag{2.19}$$

The range difference measurements converted from the TDOAs, denoted by $r_{i,1}$, are modeled as

$$r_{i,1} = cd_{i,1} = r_{i,1}^o + n_{i,1}, \tag{2.20}$$

where c is the signal propagation speed, $d_{i,1} = d_i - d_1$ is the noisy TDOA measurements, and $n_{i,1}$ is the range difference error.

Substituting (2.18) and (2.19) into (2.20) yields

$$r_{i,1} + \sqrt{(x^o - x_1)^2 + (y^o - y_1)^2} = \sqrt{(x^o - x_i)^2 + (y^o - y_i)^2} + n_{i,1},\ i = 2, 3, \cdots, M. \quad (2.21)$$

Squaring both sides of (2.21) and introducing an additional variable

$$K_1 = r_1^o = \sqrt{(x^o - x_1)^2 + (y^o - y_1)^2}. \quad (2.22)$$

We obtain

$$(x_i - x_1)(x^o - x_1) + (y_i - y_1)(y^o - y_1) + r_{i,1}K_1 = 0.5[(x_i - x_1)^2 + (y_i - y_1)^2 - r_{i,1}^2] + w_{i,1}, i = 2, 3, \cdots, M, \quad (2.23)$$

where $w_{i,1} = r_i n_{i,1} + 0.5 n_{i,1}^2$. Write (2.23) in the following matrix form,

$$\mathbf{m} = \mathbf{G}\boldsymbol{\theta} + \mathbf{w}, \quad (2.24)$$

where

$$\mathbf{m} = 0.5 \begin{bmatrix} r_{2,1}^2 - (x_2 - x_1)^2 - (y_2 - y_1)^2 \\ \vdots \\ r_{M,1}^2 - (x_M - x_1)^2 - (y_M - y_1)^2 \end{bmatrix}, \quad (2.25)$$

$$\mathbf{G} = - \begin{bmatrix} x_2 - x_1 & y_2 - y_1 & r_{2,1} \\ \vdots & \vdots & \vdots \\ x_M - x_1 & y_M - y_1 & r_{M,1} \end{bmatrix}, \quad (2.26)$$

$$\boldsymbol{\theta} = [x - x_1, y - y_1, K_1]^T, \tag{2.27}$$

$$\mathbf{w} = [w_{2,1} \cdots w_{M,1}]^T. \tag{2.28}$$

The unknown $\boldsymbol{\theta}$ is determined from

$$\hat{\boldsymbol{\theta}} = \arg\min_{\tilde{\boldsymbol{\theta}}} J(\tilde{\boldsymbol{\theta}}) = \arg\min_{\tilde{\boldsymbol{\theta}}} (\mathbf{G}\tilde{\boldsymbol{\theta}} - \mathbf{m})^T \mathbf{W} (\mathbf{G}\tilde{\boldsymbol{\theta}} - \mathbf{m}), \tag{2.29}$$

$$s.t.\ \tilde{\boldsymbol{\theta}}^T \mathbf{Z} \tilde{\boldsymbol{\theta}} = (\tilde{x} - x_1)^2 + (\tilde{y} - y_1)^2 - \tilde{K}_1^2 = 0, \tag{2.30}$$

where $\tilde{\boldsymbol{\theta}} = [\tilde{x} - x_1, \tilde{y} - y_1, \tilde{K}_1]^T$ is an optimatization variable vector, $\hat{\boldsymbol{\theta}}$ is the estimate of $\boldsymbol{\theta}$, $\mathbf{Z} = diag(1, 1, -1)$, and $\mathbf{W} = E[\mathbf{w}\mathbf{w}^T]^{-1}$ is the weighting matrix. The weighted LS solution that minimizes (2.29) is [44]

$$\hat{\boldsymbol{\theta}} = (\mathbf{G}^T \mathbf{W} \mathbf{G})^{-1} \mathbf{G}^T \mathbf{W} \mathbf{m}. \tag{2.31}$$

The second weighted least squares step is to utilize the relationship in (2.30) and refine the estimate. By squaring the elements in $\hat{\boldsymbol{\theta}}$ and rewriting (2.30), we can get another set of equations

$$\mathbf{m}_1 = \mathbf{G}_1 \boldsymbol{\theta}_1 + \mathbf{w}_1, \tag{2.32}$$

where

$$\boldsymbol{\theta}_1 = [(x - x_1)^2,\ (y - y_1)^2]^T, \tag{2.33}$$

$$\mathbf{m}_1 = [\hat{\boldsymbol{\theta}}(1)^2, \hat{\boldsymbol{\theta}}(2)^2, \hat{\boldsymbol{\theta}}(3)^2]^T, \tag{2.34}$$

$$\mathbf{G}_1 = \begin{bmatrix} 1 & 0 \\ 0 & 1 \\ 1 & 1 \end{bmatrix}. \tag{2.35}$$

The weighted least squares solution of (2.32) is

$$\hat{\boldsymbol{\theta}}_1 = (\mathbf{G}_1^T \mathbf{W}_1 \mathbf{G}_1)^{-1} \mathbf{G}_1^T \mathbf{W}_1 \mathbf{m}_1, \tag{2.36}$$

where $\mathbf{W}_1 = (E[\mathbf{w}_1 \mathbf{w}_1^T])^{-1}$ is the weighting matrix.

The final solution $\boldsymbol{\theta}_2 = [x,\ y]^T$ is simply given by the square root of $\hat{\boldsymbol{\theta}}_1$, and the sign of $\hat{\boldsymbol{\theta}}$ is retained,

$$\hat{\boldsymbol{\theta}}_2 = \mathbf{P}\sqrt{\hat{\boldsymbol{\theta}}_1} + \mathbf{x}_1, \quad \mathbf{P} = diag[sgn(\hat{\boldsymbol{\theta}}), sgn(\hat{\boldsymbol{\theta}})]. \tag{2.37}$$

Example 2.2. Repeat the test in Example 2.1 using the Chan-Ho method. As shown in Figure 9, under non-LER scenario, Chan-Ho is able to reach the CRLB at small TDOA measurement noise.

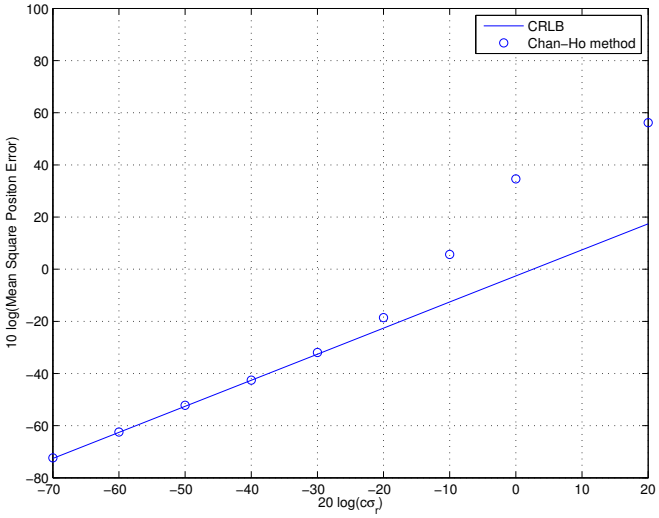

Figure 9: Source localization performance using the Chan-Ho method under the non-LER scenario

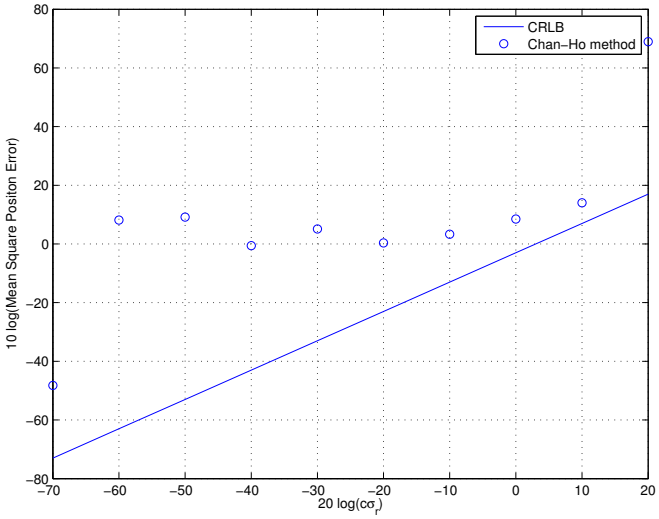

Figure 10: Source localization performance using the Chan-Ho method under the LER scenario

Example 2.3. Consider a 2-D geometry of $M = 4$ sensors with known coordinates at $(5,5)^T$,$(-5,5)^T$,$(5,-5)^T$ and $(-5,-5)^T$, while the unknown source position

is $(0.1, 0.1)^T$. The range difference noise power $c^2\sigma^2$ varies from 10^{-7} to 10^2. Note that sensors form a UCA and the source is very close to the center of the UCA, therefore the sensors have approximately equal distance to the source. Thus the geometry is sufficiently LER scenario. 2000 ensemble runs are performed.

Due to the ill-conditioned measurement matrix (see Equation 2.26) under LER scenario, the performance of Chan-Ho method has a significant degradation.

2.4.2 Separated Constrained Weighted Least Squares (SCWLS)

The separated constrained weighted least squares (SCWLS) is another method proposed in [34] to circumvent the singularity problem in LER conditions, where the sensor geometry is close to a uniform circular array and the source is close to the array center. The main strategy is to separate the source coordinates and the additional variable to different sides of the linear equations where the latter is first solved via a quadratic equation [34].

In [45], (2.29)(2.30) are solved by minimizing the Lagrangian:

$$L(\tilde{\boldsymbol{\theta}}, \lambda) = (\mathbf{G}\tilde{\boldsymbol{\theta}} - \mathbf{m})^T \mathbf{W} (\mathbf{G}\tilde{\boldsymbol{\theta}} - \mathbf{m}) + \lambda \tilde{\boldsymbol{\theta}}^T \mathbf{Z} \tilde{\boldsymbol{\theta}}, \tag{2.38}$$

where λ is the Lagrange multiplier. The constrained weighted least squares (CWLS) solution is

$$\tilde{\boldsymbol{\theta}}_{CWLS} = (\mathbf{G}^T \mathbf{W} \mathbf{G} + \lambda \mathbf{Z})^{-1} \mathbf{G}^T \mathbf{W} \mathbf{m}, \tag{2.39}$$

where λ is a root of the 4th order polynomial [45]:

$$\sum_{i=1}^{3} \frac{u_i v_i}{(\lambda + \zeta_i)^2} = 0, \tag{2.40}$$

with $[u_1, u_2, u_3]^T = \mathbf{U}^T\mathbf{Z}\mathbf{G}^T\mathbf{W}\mathbf{m}$, $[v_1, v_2, v_3]^T = \mathbf{U}^{-1}\mathbf{G}^T\mathbf{W}\mathbf{m}$ and $\mathbf{G}^T\mathbf{W}\mathbf{G}\mathbf{Z}$ $=\mathbf{U}\text{diag}(\zeta_1, \zeta_2, \zeta_3)\mathbf{U}^{-1}$. To fix the matrix ill-conditioned problem in (2.39), (2.24) is expressed as

$$\mathbf{m} - \mathbf{g}K_1 = \mathbf{A}\boldsymbol{\eta} + \mathbf{w}, \tag{2.41}$$

where $\mathbf{A} = [[\mathbf{G}]_{:,1}, [\mathbf{G}]_{:,2}]$ and $\mathbf{g} = [\mathbf{G}]_{:,3}$ with$[\mathbf{G}]_{:,i}$ being the ith column of the matrix $\mathbf{G}$ and $\boldsymbol{\eta} = [[\boldsymbol{\theta}]_1, [\boldsymbol{\theta}]_2]^T$ with $[\theta]_i$ being the ith element of the vector θ.

The SCWLS position estimate $\hat{\boldsymbol{\eta}}$ is the $\tilde{\boldsymbol{\eta}}$ that minimizes the cost function $J(\tilde{\boldsymbol{\eta}}, \tilde{K}_1)$,

$$\hat{\boldsymbol{\eta}} = \arg\min_{\tilde{\boldsymbol{\eta}}} J(\tilde{\boldsymbol{\eta}}, \tilde{K}_1) = \arg\min_{\tilde{\boldsymbol{\eta}}} (\mathbf{A}\tilde{\boldsymbol{\eta}} - \mathbf{m} + \mathbf{g}\tilde{K}_1)^T\mathbf{W}(\mathbf{A}\tilde{\boldsymbol{\eta}} - \mathbf{m} + \mathbf{g}\tilde{K}_1), \tag{2.42}$$

$$s.t.\ \tilde{\boldsymbol{\eta}}^T\tilde{\boldsymbol{\eta}} = \tilde{K}_1^2, \tag{2.43}$$

where $\tilde{\boldsymbol{\eta}} = [[\tilde{\boldsymbol{\theta}}]_1, [\tilde{\boldsymbol{\theta}}]_2]^T$ is the optimization variable for $\boldsymbol{\eta}$. Solving the SCWLS problem in (2.42) and (2.43) is equivalent to minimizing the Lagrangian:

$$L(\tilde{\boldsymbol{\eta}}, \beta, \tilde{K}_1) = (\mathbf{A}\tilde{\boldsymbol{\eta}} - \mathbf{m} + \mathbf{g}\tilde{K}_1)^T\mathbf{W}(\mathbf{A}\tilde{\boldsymbol{\eta}} - \mathbf{m} + \mathbf{g}\tilde{K}_1) + \beta(\tilde{\boldsymbol{\eta}}^T\tilde{\boldsymbol{\eta}} - \tilde{K}_1^2), \tag{2.44}$$

where β is the Lagrange multiplier and equal to λ.

The minimum of (2.44) is found by differentiating $L(\tilde{\boldsymbol{\eta}}, \beta, \tilde{K}_1)$ with respect to $\tilde{\boldsymbol{\eta}}$

and $\tilde{K}_1$ respectively. By setting the derivatives to zero, we get

$$\hat{\boldsymbol{\eta}} = (\mathbf{A}^T\mathbf{W}\mathbf{A} + \beta\mathbf{I}_2)^{-1}(\mathbf{A}^T\mathbf{W}\mathbf{m} - \mathbf{A}^T\mathbf{W}\mathbf{g}\hat{K}_1) \tag{2.45}$$

and

$$\hat{K}_1 = \frac{\mathbf{g}^T\mathbf{W}\mathbf{A}\hat{\boldsymbol{\eta}} - \mathbf{g}^T\mathbf{W}\mathbf{m}}{\beta - \mathbf{g}^T\mathbf{W}\mathbf{g}}. \tag{2.46}$$

Substituting (2.45) into the equality constraint of (2.43) results in a quadratic equation

$$a\hat{K}_1^2 + b\hat{K}_1 + c = 0, \tag{2.47}$$

where $a = (\mathbf{A}^T\mathbf{W}\mathbf{g})^T(\mathbf{A}^T\mathbf{W}\mathbf{A} + \beta\mathbf{I}_2)^{-2}\mathbf{A}^T\mathbf{W}\mathbf{g} - 1$, $b = -2(\mathbf{A}^T\mathbf{W}\mathbf{m})^T(\mathbf{A}^T\mathbf{W}\mathbf{A} + \beta\mathbf{I}_2)^{-2}\mathbf{A}^T\mathbf{W}\mathbf{g}$ and $c = (\mathbf{A}^T\mathbf{W}\mathbf{m})^T(\mathbf{A}^T\mathbf{W}\mathbf{A} + \beta\mathbf{I}_2)^{-2}\mathbf{A}^T\mathbf{W}\mathbf{m}$. After solving $\beta, \hat{K}_1$ and $\hat{\boldsymbol{\eta}}$, we will choose the set of $(\beta, \hat{K}_1, \hat{\boldsymbol{\eta}})$ that minimizes the cost function $J(\tilde{\boldsymbol{\eta}}, \tilde{K}_1)$. The detailed root selection for $\tilde{K}_1$ is referred to [45].

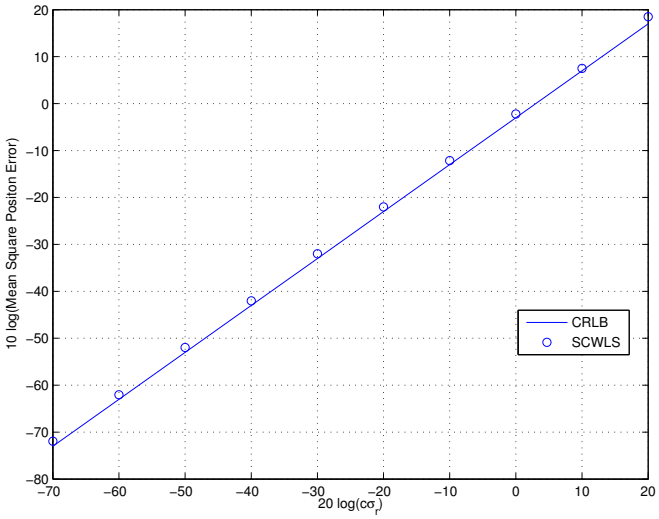

Figure 11: Source localization performance using the SCWLS method under the LER scenario

Example 2.4. Repeat the test in Example 2.3 using the SCWLS method. As shown in Figure 11, SCWLS is able to achieve the CRLB at the given TDOA noise power levels.

2.4.3 Dual-root Minimum Variance Least Squares (DMVLS)

Romero and Mason *et al.* [46] analyze and test over a wide range of noise levels some of the most popular algorithms for solving overdetermined systems of the time of arrival (TOA) or pseudo range geolocation equations. They point out several factors that should be taken into account when judging the performance of TOA algorithms. On such factor is the large equal radius (LER) condition [33], where certain algorithms encounter a singularity that is referred to as the reduced least squares (RLS) singularity, even if the geometric dilution of precision (GDOP) is not bad.

They propose the dual-root minimum variance least squares (DMVLS) method to fit the LER conditions. The method is summarized in this section. Based on the localization scenario in Section 2.1, similar to (2.18), the range from the true source to the ith sensor is modeled as

$$\|\mathbf{u}^o - \mathbf{s}_i\| = \tau_i^o - \tau, i = 1, 2, \cdots, M, \tag{2.48}$$

where τ_i^o is the noise less pseudo range with sensor i, and τ is the range-equivalent receiver clock bias. Square both sides

$$\|\mathbf{u}^o - \mathbf{s}_i\|^2 = (\tau_i^o - \tau)^2, i = 1, 2, \cdots, M. \tag{2.49}$$

Let $\mathbf{x}$ to be the unknown source location. We can rewrite (2.42) as

$$\mathbf{m} = \mathbf{G}\boldsymbol{\theta} + \mu\mathbf{e}, \tag{2.50}$$

where

$$\boldsymbol{\theta} = (\mathbf{x}^T, \tau)^T, \tag{2.51}$$

$$\mu = \boldsymbol{\theta}^T\mathbf{L}\boldsymbol{\theta} = \mathbf{x}^T\mathbf{x} - \tau^2, \tag{2.52}$$

$$\mathbf{L} = \begin{bmatrix} \mathbf{I} & \mathbf{0} \\ \mathbf{0} & -1 \end{bmatrix}, \tag{2.53}$$

$$\mathbf{G} = \begin{bmatrix} -2\mathbf{s}_1^T & 2\tau_1 \\ -2\mathbf{s}_2^T & 2\tau_2 \\ \vdots & \vdots \\ -2\mathbf{s}_M^T & 2\tau_M \end{bmatrix}, \tag{2.54}$$

and defining

$$\mathbf{e} = (1, 1, \cdots, 1)^T, \tag{2.55}$$

$$\mathbf{m}^T = (m_1, m_2, \cdots, m_M), m_i = \tau_i^2 - \mathbf{s}_i^T\mathbf{s}_i. \tag{2.56}$$

Ideally we would like to satisfy the system of equations

$$\gamma(\boldsymbol{\theta}) = \mathbf{G}\boldsymbol{\theta} + \mu\mathbf{e} - \mathbf{m} = \mathbf{0}. \tag{2.57}$$

We will get a minimum variance solution by minimizing the objective function

$$P(\boldsymbol{\theta}) = \frac{1}{2}\gamma(\boldsymbol{\theta})^T \mathbf{W}\gamma(\boldsymbol{\theta}), \tag{2.58}$$

where $\mathbf{W}$ is the optimal weighting matrix. When the gradient of $P(\boldsymbol{\theta})$ vanishes, we get

$$\boldsymbol{\Gamma}^T \mathbf{W}\gamma(\boldsymbol{\theta}) = \mathbf{0}, \tag{2.59}$$

where

$$\boldsymbol{\Gamma} = \mathbf{G} + 2\mathbf{e}\boldsymbol{\theta}^T \mathbf{L}. \tag{2.60}$$

Since $\boldsymbol{\Gamma}$ contains the true source location $\mathbf{x}$, which is not available in practice, $\boldsymbol{\theta}$ is replaced by the estimate $\hat{\boldsymbol{\theta}}$ using a consistent but non MV technique such as RLS algorithm. Please note all the DMVLS simulation results we perform, $\hat{\boldsymbol{\theta}}$ is set to be the true source position.

We solve the DMVLS equations in almost identical way as solving Bancroft equations [29]. $\boldsymbol{\theta}$ can be determined by solving a quadratic equation for $\mu = \boldsymbol{\theta}^T \mathbf{L}\boldsymbol{\theta}$. The solution to (2.59) can be written as

$$\boldsymbol{\theta} = \mu\boldsymbol{\alpha} + \boldsymbol{\beta}, \tag{2.61}$$

where

$$\boldsymbol{\alpha} = (\boldsymbol{\Gamma}^T \mathbf{W}\boldsymbol{\Gamma})^{-1}\boldsymbol{\Gamma}^T \mathbf{W}\mathbf{e}, \quad \boldsymbol{\beta} = (\boldsymbol{\Gamma}^T \mathbf{W}\boldsymbol{\Gamma})^{-1}\boldsymbol{\Gamma}^T \mathbf{W}\mathbf{m}. \tag{2.62}$$

Substituting the expression in (2.61) into Equation (2.52), we get a quadratic equation for μ. The two roots of this quadratic when substituted back into (2.61) give two roots of the DMVLS algorithm. One root will solve the localization problem for user

position and clock offset. To distinguish the actual solution, we subtitle the roots back into the Equation (2.48) defining the original pseudoranges and choose the root that minimizes the cost function $\mathbf{J}(\hat{\mathbf{t}})$ according to the noisy version of Equation (2.48)

$$\mathbf{J}(\hat{\mathbf{t}}) = (\hat{\mathbf{t}} - \boldsymbol{\tau})^T \mathbf{W} (\hat{\mathbf{t}} - \boldsymbol{\tau}), \tag{2.63}$$

where $\hat{\mathbf{t}} = (\|\hat{\mathbf{x}} - \mathbf{s}_1\| + \hat{\tau}, \|\hat{\mathbf{x}} - \mathbf{s}_2\| + \hat{\tau}, \cdots, \|\hat{\mathbf{x}} - \mathbf{s}_M\| + \hat{\tau})^T$ is the event time vector and $\boldsymbol{\tau} = [\tau_1, \tau_2, \cdots, \tau_M]^T$.

Example 2.5. Repeat the test in Example 2.3 using the DMVLS method. As shown in Figure 12, DMVLS has comparable performance with the SCWLS, and it has a threshold effect when the TOA noise power is greater than 10.

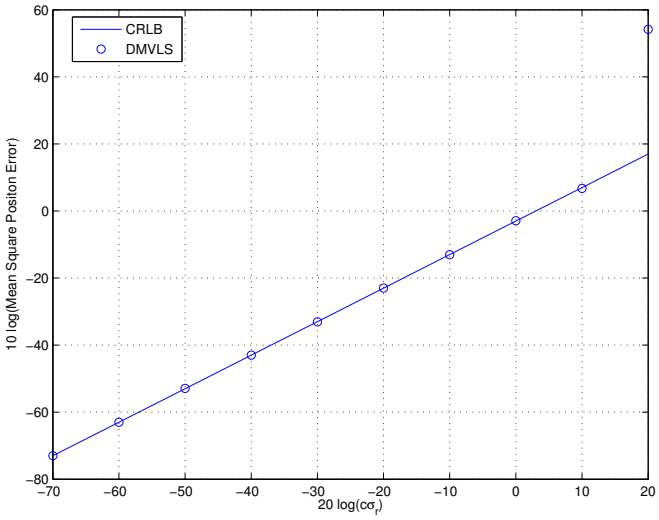

Figure 12: Source localization performance using the DMVLS method under the LER scenario

2.5 Conclusion

In this chapter, theoretical estimation accuracy for source localization, CRLB, and its computation are addressed. We have addressed the nonlinear approach ML and the linear approach LLS for determining the source location. The nonlinear approach solves the nonlinear equation directly constructed from TDOA, TDOA, AOA and RSS measurements, while the linear methodology convert the nonlinear location equations to be linear. LLS is widely used due to computation efficiency, and we introduced the classical two-step LLS method proposed by Chan and Ho, and the other two LLS algorithms, DMVLS and SCWLS, which are proposed to solve the LER geolocation problems. Examples of localization using ML, Chan-Ho method, DMVLS and SCWLS as well as their performance comparison with CRLBs are provided. Under the given LER scenario, the Chan-Ho method has a great performance degradation due to the ill-conditioned measurement matrix, whereas SCWLS and DMVLS can reach the CRLB.

Chapter 3

Proposed Method in Two-dimensional Space

In this section, we first illustrate the typical LER scenario in two dimensional space, followed by the development of the proposed method based on TDOA measurements. We then analyze the performance theoretically and perform simulations to confirm the theoretical development. The performance of the proposed method in 2-D is also compared with Chan-Ho [18], SCWLS [45] and DMVLS [46] through simulations.

In the presence of sensor position error, we give the CRLB and MSE analysis theoretically and develop a modified estimator that would take into account the sensor position errors and eventually improve the source location estimation accuracy. Simulation result is presented to confirm the theoretical analysis.

3.1 LER Localization Scenario in 2-D

Consider one source and $M \geq 3$ sensors in a two-dimensional space as shown in Figure 13, where the sensor geometry is close to a uniform circular array (UCA) and the source is located at or near the center. Let $\{*\}^o$ denote the noise-free quantity of $\{*\}$. The true source location $\mathbf{u}^o = [x^o, y^o]^T$ is unknown to be estimated using the TDOAs of the source signal received at the sensors. Let $\mathbf{s}_i^o = [x_i^o, y_i^o]^T$ be the true ith sensor position. The angles of the true source and the ith sensor locations with respect to the x-axis are denoted by α^o and α_i^o respectively.

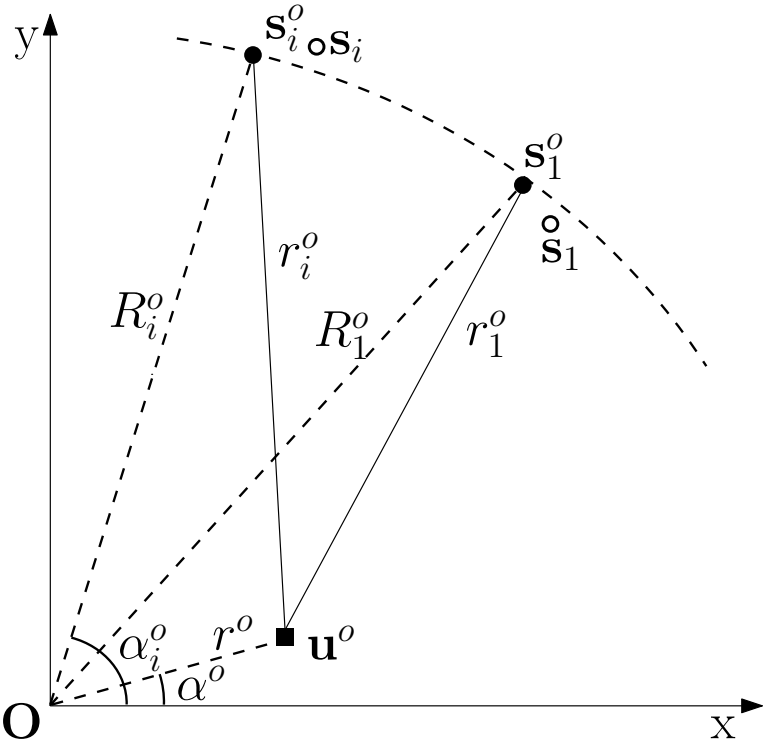

Figure 13: Illustration of the sensor geometry under 2-D LER conditions. Solid disks denote the true sensor positions that are not known and open circles denote the available sensor positions that are erroneous.

The true range between the source and the ith sensor is

$$r_i^o = \|\mathbf{u}^o - \mathbf{s}_i^o\| = \sqrt{(x^o - x_i^o)^2 + (y^o - y_i^o)^2}. \tag{3.1}$$

The distance between the origin and the ith sensor is

$$R_i^o = \|\mathbf{s}_i^o\| = \sqrt{x_i^{o2} + y_i^{o2}}. \tag{3.2}$$

And the distance between the origin and the source, referred as the source range, is

$$r^o = \|\mathbf{u}^o\| = \sqrt{x^{o2} + y^{o2}}. \tag{3.3}$$

The true range difference measurements from TDOAs, denoted by r_{i1}^o, are modeled as

$$r_{i1}^o = cd_{i1}^o = r_i^o - r_1^o = r_{i1} - n_{ri}, \tag{3.4}$$

where d_{i1}^o denote the true TDOA of a signal received by the sensor pair i and 1, c is the signal propagation speed, and n_{ri} is the range difference measurement noise. Collecting the TDOA measurements in the matrix form yields

$$\mathbf{r}^o = \mathbf{r} - \mathbf{n}_r, \tag{3.5}$$

where $\mathbf{r}^o = [r_{21}^o, r_{31}^o, \cdots, r_{M1}^o]^T$. The range difference measurement noise vector $\mathbf{n}_r = [n_{r2}, \cdots, n_{rM}]^T$ is assumed a zero-mean Gaussian random vector, and has an $(M-1) \times (M-1)$ covariance matrix $\mathbf{Q}_r$.

In the absence of sensor position errors, we assume the available sensor locations

$\mathbf{s}_i = [x_i, y_i]^T, i = 1, 2, \cdots, M$ are the same as the true sensor locations $\mathbf{s}_i^o$, so as the ith sensor range $R_i^o = R_i$.

In the presence of sensor position errors, the available sensor positions $\mathbf{s}_i$ are erroneous and the true sensor positions $\mathbf{s}_i^o$ are unknown. The available sensor positions can be modeled as

$$\mathbf{s}_i = \mathbf{s}_i^o + \mathbf{n}_{si} \tag{3.6}$$

where $\mathbf{n}_{si}$ represents the position error for sensor i and $\mathbf{n}_s = [\mathbf{n}_{s1}^T, \mathbf{n}_{s2}^T, \cdots, \mathbf{n}_{sM}^T]^T$ is also modeled as a zero-mean Gaussian random with covariance matrix $\mathbf{Q}_s$.

3.2 Closed-form Solution in the Absence of Sensor Position Errors

3.2.1 Algorithm Development

In the absence of sensor position error, we assume $\mathbf{s}_i = \mathbf{s}_i^o$ and $R_i^o = R_i$. According to the Law of Cosines, in the triangle formed by the origin, $\mathbf{u}^o$ and $\mathbf{s}_i$, we have

$$\begin{aligned} r_i^{o2} &= R_i^2 + r^{o2} - 2R_i r^o \cos(\alpha_i - \alpha^o) \\ &= R_i^2[1 + \frac{r^{o2}}{R_i^2} - 2\frac{r^o}{R_i}\cos(\alpha_i - \alpha^o)]. \end{aligned} \tag{3.7}$$

Using the Taylor series expansion up to linear term, we can approximate r_i^o by

$$\begin{aligned} r_i^o &\simeq R_i[1 + \frac{r^{o2}}{2R_i^2} - \frac{r^o}{R_i}\cos(\alpha_i - \alpha^o)] \\ &= R_i + \frac{r^{o2}}{2R_i} - r^o(\cos\alpha_i \cos\alpha^o + \sin\alpha_i \sin\alpha^o). \end{aligned} \tag{3.8}$$

Substitute (3.8) into (3.4) and let $R_{i1} = R_i - R_1$, then we have

$$r_{i1}^o - R_{i1} = (r^o \cos\alpha^o)(\cos\alpha_1 - \cos\alpha_i) + (r^o \sin\alpha^o)(\sin\alpha_1 - \sin\alpha_i), \tag{3.9}$$

while $\frac{r^{o2}}{2}(\frac{1}{R_i} - \frac{1}{R_1}) \approx 0$ when $R_i \gg r^o$. Let $\boldsymbol{\theta} = [r\cos\alpha, r\sin\alpha]^T = [x, y]^T$. With noisy TDOA measurements, replacing r_{i1}^o by $r_{i1} - n_{ri}$, the equation error of (3.9) can be expressed in the matrix form as

$$\mathbf{n}_r = \mathbf{h} - \mathbf{G}\boldsymbol{\theta}^o, \tag{3.10}$$

where

$$\mathbf{G} = \begin{bmatrix} \cos\alpha_1 - \cos\alpha_2 & \sin\alpha_1 - \sin\alpha_2 \\ \vdots & \vdots \\ \cos\alpha_1 - \cos\alpha_M & \sin\alpha_1 - \sin\alpha_M \end{bmatrix}, \mathbf{h} = \begin{bmatrix} r_{21} - R_{21} \\ \vdots \\ r_{M1} - R_{M1} \end{bmatrix}, \tag{3.11}$$

and $\mathbf{n}_r = [n_{r2}, n_{r3}, \cdots, n_{rM}]^T$ is the range difference measurement noise vector. The weighted LS solution is

$$\hat{\boldsymbol{\theta}} = (\mathbf{G}^T\mathbf{W}\mathbf{G})^{-1}\mathbf{G}^T\mathbf{W}\mathbf{h}, \tag{3.12}$$

where $\mathbf{W} = \mathbf{Q}_r^{-1}$ is the weighting matrix.

An iterative method is applied due to the Taylor series expansion. Here $\mathbf{O}^k$ denotes the origin used in the kth iteration and $\hat{\boldsymbol{\theta}}^k$ is the estimate of the kth iteration, $k \geq 1$.

- Initialize the $\mathbf{O}^1$ as $(0, 0)^T$
- Iteration
    1. Estimate $\hat{\boldsymbol{\theta}}$ with Equation (3.12)

2. if $k > 1$

   (a) If $\left\|\hat{\boldsymbol{\theta}}^{k}\right\| > \left\|\hat{\boldsymbol{\theta}}^{k-1}\right\|$, stop, solution= $\hat{\boldsymbol{\theta}}^{k-1} + \mathbf{O}^{k-1}$;

   (b) else if $\left\|\hat{\boldsymbol{\theta}}^{k}\right\| < \varepsilon_{\hat{\boldsymbol{\theta}}}$, stop, solution= $\hat{\boldsymbol{\theta}}^{k} + \mathbf{O}^{k}$; end

3. Set $\mathbf{O}^{k+1} = \hat{\boldsymbol{\theta}}^{k} + \mathbf{O}^{k}$, go to step 1

- Until a preset number of iterations is reached or until convergence

It is found by simulations 5 iterations are enough to reach convergence in most cases. When the TDOA noise power is large, the solution may not converge at all. Through step (a), we can check the divergence and stop iterations before the solution diverges.

3.2.2 Comparison with CRLB and Bias Analysis

The CRLB is the lowest possible variance that an estimator can reach, which is defined as the inverse of the Fisher information matrix FIM [44]. Let $\mathbf{r}$ denote the range difference measurement vector from TDOAs, FIM can be expressed by

$$\text{FIM} = E\Big[\Big(\frac{\partial \ln p(\mathbf{r};\boldsymbol{\theta})}{\partial \boldsymbol{\theta}}\Big)\Big(\frac{\partial \ln p(\mathbf{r};\boldsymbol{\theta})}{\partial \boldsymbol{\theta}}\Big)^{T}\Big]\Big|_{\boldsymbol{\theta}=\boldsymbol{\theta}^{o}}. \tag{3.13}$$

Assuming Gaussian TDOA noise, $p(\mathbf{r};\boldsymbol{\theta})$ is Gaussian with mean $\mathbf{r}^{o}$ and covariance matrix $\mathbf{Q}_{r}$. Taking natural log and performing differentiation yields

$$\text{CRLB} = \text{cov}(\boldsymbol{\theta}^{o})_{min} = \text{FIM}^{-1} = \Big(\frac{\partial \mathbf{r}^{oT}}{\partial \boldsymbol{\theta}}\mathbf{Q}_{r}^{-1}\frac{\partial \mathbf{r}^{o}}{\partial \boldsymbol{\theta}^{T}}\Big)^{-1}\Big|_{\boldsymbol{\theta}=\boldsymbol{\theta}^{o}}, \tag{3.14}$$

where the partial derivative is found to be

$$\frac{\partial \mathbf{r}^o}{\partial \boldsymbol{\theta}^T}|_{\boldsymbol{\theta}=\boldsymbol{\theta}^o} = \begin{bmatrix} \frac{x_1-x^o}{r_1^o} - \frac{x_2-x^o}{r_2^o} & \frac{y_1-y^o}{r_1^o} - \frac{y_2-y^o}{r_M^o} \\ \vdots & \vdots \\ \frac{x_1-x^o}{r_1^o} - \frac{x_M-x^o}{r_M^o} & \frac{y_1-y^o}{r_1^o} - \frac{y_M-y^o}{r_M^o} \end{bmatrix}. \tag{3.15}$$

The covariance matrix of $\boldsymbol{\theta}^o$ is [44]

$$\text{cov}(\boldsymbol{\theta}^o) = (\mathbf{G}^T\mathbf{W}\mathbf{G})^{-1}, \tag{3.16}$$

where $\mathbf{G}$ can be rewritten as

$$\mathbf{G} = \begin{bmatrix} \frac{x_1}{R_1} - \frac{x_2}{R_2} & \frac{y_1}{R_1} - \frac{y_2}{R_M} \\ \vdots & \vdots \\ \frac{x_1}{R_1} - \frac{x_M}{R_M} & \frac{y_1}{R_1} - \frac{y_M}{R_M} \end{bmatrix}. \tag{3.17}$$

In the 2-D LER conditions, $R_i \gg r^o$, $R_i \simeq r_i^o$

$$\frac{x^o}{r_i^o} \simeq \frac{x^o}{R_i} \leq \frac{r^o}{R_i} \simeq 0, \tag{3.18}$$

accordingly,

$$\frac{x_i}{R_i} \simeq \frac{x_i - x^o}{r_i^o}. \tag{3.19}$$

Similarly

$$\frac{y_i}{R_i} \simeq \frac{y_i - y^o}{r_i^o}. \tag{3.20}$$

Therefore

$$\mathbf{G} \simeq \left.\frac{\partial \mathbf{r}^o}{\partial \boldsymbol{\theta}^T}\right|_{\boldsymbol{\theta}=\boldsymbol{\theta}^o}, \tag{3.21}$$

the proposed estimator is able to achieve the optimum performance CRLB when LER is sufficiently satisfied in 2-D.

The bias of the proposed estimator comes from the inaccuracy of the Taylor series expansion in (3.8). $\Delta\{*\}$ is used to denote the noise component in $\{*\}$. Upon substituting $\mathbf{G} = \mathbf{G}^o$, $\mathbf{h} = \mathbf{n}_r + \mathbf{h}^o$ and $\boldsymbol{\theta} = \Delta\boldsymbol{\theta} + \boldsymbol{\theta}^o$ to (3.12), we have

$$\begin{aligned} \Delta\boldsymbol{\theta} &= (\mathbf{G}^T\mathbf{W}\mathbf{G})^{-1}\mathbf{G}^T\mathbf{W}(\mathbf{h} - \mathbf{G}\boldsymbol{\theta}^o) \\ &= (\mathbf{G}^T\mathbf{W}\mathbf{G})^{-1}\mathbf{G}^T\mathbf{W}(\mathbf{n}_r + \mathbf{h}^o - \mathbf{G}\boldsymbol{\theta}^o). \end{aligned} \tag{3.22}$$

Let $\mathbf{b} = (\mathbf{G}^T\mathbf{W}\mathbf{G})^{-1}\mathbf{G}^T\mathbf{W}(\mathbf{h}^o - \mathbf{G}\boldsymbol{\theta}^o)$ denote the bias component. The mean square error (MSE) is expressed as

$$\mathrm{MSE}(\boldsymbol{\theta}) = E[\Delta\boldsymbol{\theta}^T\Delta\boldsymbol{\theta}] = \mathrm{cov}(\boldsymbol{\theta}^o) + \mathbf{b}^T\mathbf{b}. \tag{3.23}$$

When the range ratio is large, the value of the bias from the Taylor series expansion is ignorable and the proposed estimator is able to reach the CRLB in a wide range of TDOA measurement noise. But when the noise power is small, the bias term is dominant in MSE. To reduce the bias, we apply the iterations and update the origin to create the sufficient LER situations where the bias value is ignorable. In relatively large noise regions, the covariance is dominant and the matrix $\mathbf{G}$ is independent from TDOA measurement noises, thus the estimator can reach the optimum performance. Therefore the proposed estimator is able to achieve CRLB in a wide range of noise levels.

3.2.3 Simulations

In the LER conditions, sensors form a uniform or close to uniform circular array, and $R_i \simeq R,\ i = 1, 2, \cdots, M$, where R is the common sensor range. We define $\frac{R}{r^o}$ as the sensor range and the source range ratio (hereafter called range ratio). In this

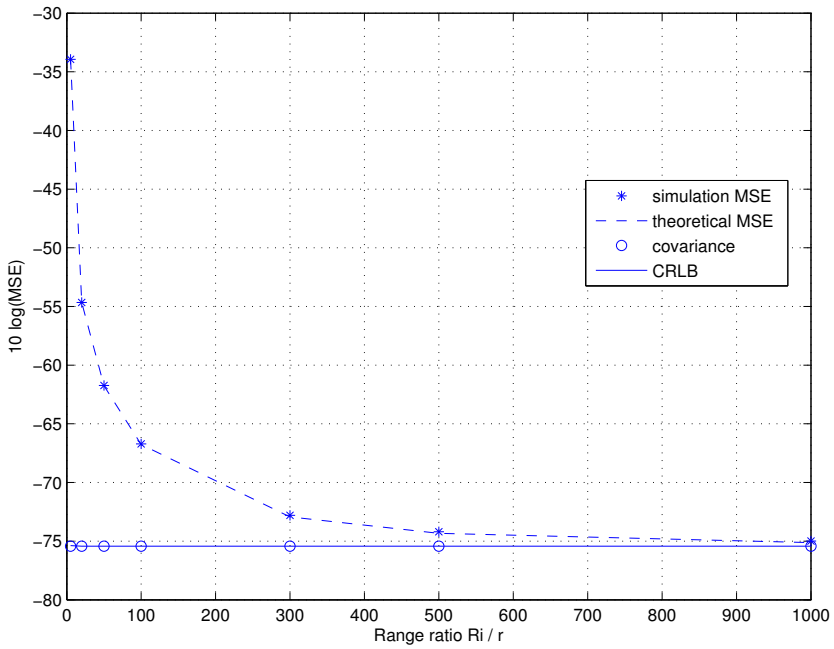

Figure 14: The bias and MSE behaviors of the proposed method in 2-D with $(c\sigma_r)^2 = 10^{-7}$

section, we will first present the bias and MSE behaviors of the proposed method when the range ratio increases, as shown in Figure 14. The simulation scenario has a uniform circular array with 7 sensors. The source range is fixed as 1 and its angle with respect to the x-axis is 50°, while the range ratio varies with the given values $[5, 20, 50, 100, 300, 500, 1000]$ respectively. The angles of the sensors with respect to the x-axis are fixed as $[0°, 50°, 100°, 150°, 200°, 250°, 300°]$. σ_r^2 denotes the TDOA measurement noise power, and the range difference measurement noise power $(c\sigma_r)^2$

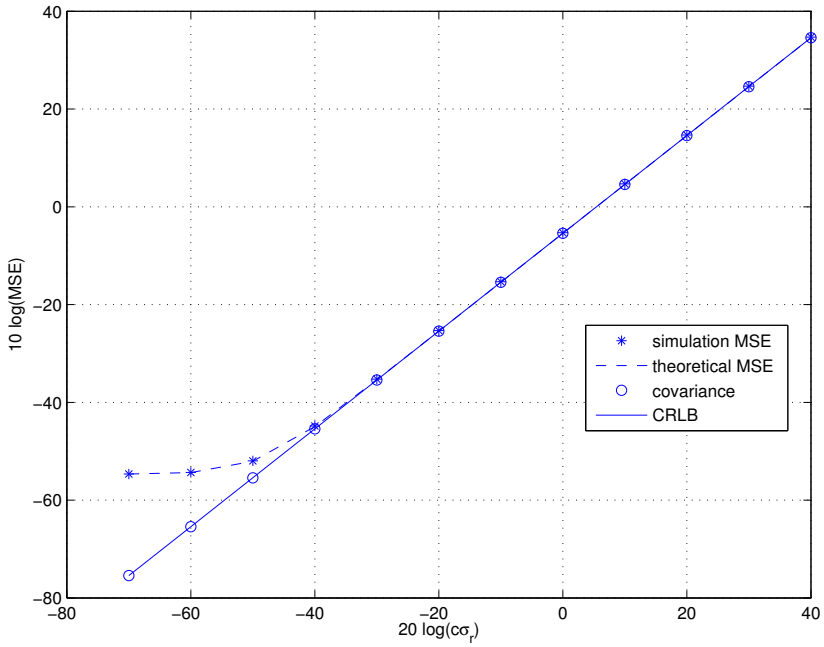

Figure 15: The bias and MSE behaviors of the proposed method in a certain 2-D geometry with the range ratio equal to 20

is fixed as 10^{-7}.

In Figure 14, we compare the simulation MSE, the theoretical MSE, covariance and CRLB. Bias corresponds to the difference between the theoretical MSE and the covariance. With the range ratio increasing, the accuracy of Taylor series expansion also improves which reduces the bias value. On the other hand, if we set $(c\sigma_r)^2$ to vary between 10^{-7} and 10^4 and fix range ratio to be 20, as shown in Figure 15, the bias component can be dominant in small noise regions, but ignorable in large noise regions.

Next we present two simulation examples to assess the relative performance of the proposed method, DMVLS, SCWLS and Chan-Ho method. In the simulations, DMVLS is initialized with the true source location. Its root selection strategy is to

choose the root that minimizes the cost function (2.63) in section 2.4.3.

Example 3.1. Sensors are randomly positioned along a uniform circle and sensor ranges are fixed to be 40. We assume there are small random fluctuations of sensor ranges between 0 and 1. The source has a randomly distributed range between 0 and 10. The angles of the source and the sensors with respect to the x-axis are randomly distributed between 0° and 360°. We perform 100 randomly distributed geometries and 1000 ensemble runs for each geometry.

Figure 16 shows the performance comparison of the proposed method, DMVLS, SCWLS and Chan-Ho method with randomly distributed 2-D geometries. In this figure, Chan-Ho method can reach CRLB in the small noise regions and it has a threshold effect around noise power 10^{-3}. The MSEs of the proposed method and SCWLS can reach CRLB in the whole given noise regions, and DMVLS has a comparable performance while its MSE has a slight deviation when the noise power is 10^3.

Table 2 shows the averaged computation time comparison for each ensemble run in 2-D randomly distributed geometries. The proposed method in 2-D is much more time efficient compared to DMVLS and SCWLS.

Table 2: Comparison of the averaged computation time for each ensemble run in 2-D randomly distributed geometries

Algorithm	The Proposed Method	Chan-Ho	DMVLS	SCWLS
Computation Time (second)	4.48×10^{-4}	3.00×10^{-4}	1.08×10^{-3}	1.88×10^{-3}

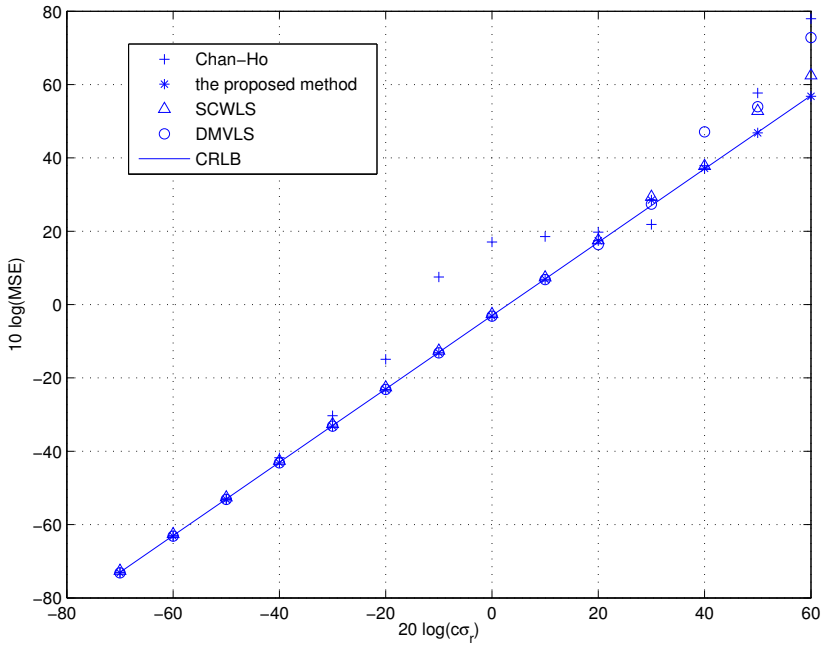

Figure 16: Performance comparison with randomly distributed 2D geometries

Example 3.2. In this example, we show the estimate results comparison from a certain 2-D LER geometry. The geometry is shown in Table 3. 2000 ensemble runs are performed. In the figure 17, Chan-Ho fails due to the ill-conditioned measurement matrix. DMVLS and SCWLS deviate from CRLB when the noise power is 1. The proposed method is able to reach CRLB in the whole given noise regions except the very small deviation when the noise power is 10.

Table 3: Geometry information of a certain 2-D LER scenario

Geometry	Range	Angle
Ture Source Location	0.4	179°
Available Source Locations	4	344°
		269°
		200°
		321°
		225°
		303°
		57°

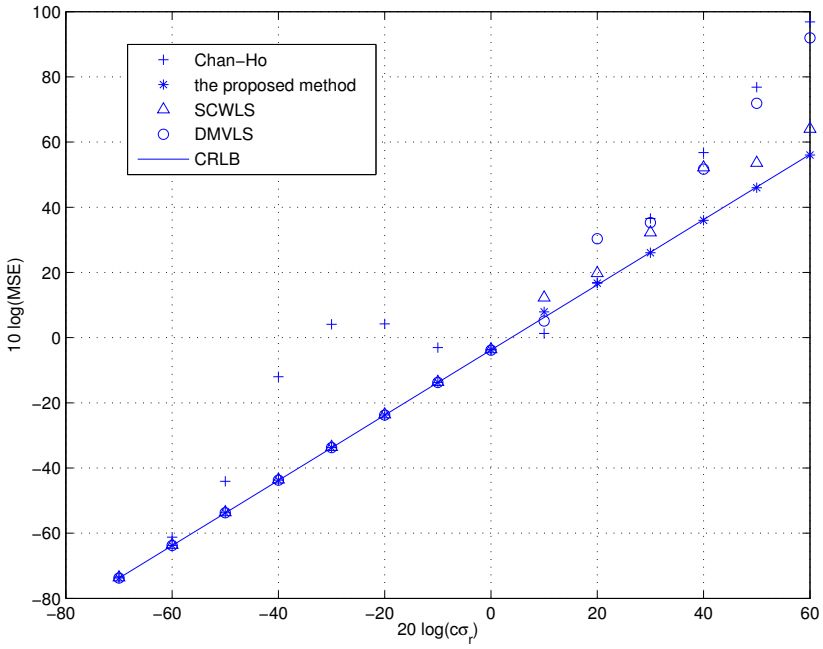

Figure 17: Performance comparison with a certain 2D geometry

3.3 Closed-form Solutions with Sensor Position Errors

The performance loss due to ignoring the sensor position error is not negligible. We shall take sensor position errors into account in the proposed estimator and eventually reduce the performance degradation caused by sensor position errors.

3.3.1 Algorithm Development

Ho *et al.* [36] has developed a closed-form solution to improve the source location estimate based on TDOA measurements. By following the general procedures in [36], first we rewrite (3.9) into a sensor position noise-free form and it gives

$$\begin{aligned} r_{i1}^o - R_{i1}^o &= (r^o \cos\alpha^o)(\cos\alpha_1^o - \cos\alpha_i^o) + (r^o \sin\alpha^o)(\sin\alpha_1^o - \sin\alpha_i^o) \\ &= x^o(\cos\alpha_1^o - \cos\alpha_i^o) + y^o(\sin\alpha_1^o - \sin\alpha_i^o),\ i = 2, 3, \cdots, M. \end{aligned} \tag{3.24}$$

The true sensor range is denoted by $R_i^o = \|\mathbf{s}_i^o\| = \|\mathbf{s}_i - \mathbf{n}_{si}\|$. Using the Taylor expansions, we can get

$$\begin{aligned} \|\mathbf{s}_i^o\| &= \|\mathbf{s}_i\| - \frac{\mathbf{s}_i^T}{\|\mathbf{s}_i\|}\mathbf{n}_{si}, \\ i.e.\ R_i^o &= R_i - \frac{\mathbf{s}_i^T}{\|\mathbf{s}_i\|}\mathbf{n}_{si},\ i = 1, 2, \cdots, M. \end{aligned} \tag{3.25}$$

Thus we can express the true sensor range difference as

$$R_{i1}^o = R_i^o - R_1^o = R_{i1} - \frac{\mathbf{s}_i^T}{\|\mathbf{s}_i\|}\mathbf{n}_{si} + \frac{\mathbf{s}_1^T}{\|\mathbf{s}_1\|}\mathbf{n}_{s1},\ i = 2, 3, \cdots, M. \tag{3.26}$$

Similarly,

$$\begin{aligned}\cos\alpha_i^o &= \frac{x_i^o}{\left\|\mathbf{s}_i^o\right\|} = \frac{x_i}{\|\mathbf{s}_i\|} - \frac{1}{\|\mathbf{s}_i\|}(\mathbf{i}_x - \frac{x_i\mathbf{s}_i}{\|\mathbf{s}_i\|^2})\mathbf{n}_{si} \\ &= \cos\alpha_i - \frac{1}{\|\mathbf{s}_i\|}(\mathbf{i}_x - \frac{x_i\mathbf{s}_i}{\|\mathbf{s}_i\|^2})\mathbf{n}_{si},\ i = 1, 2, \cdots, M,\end{aligned} \tag{3.27}$$

and

$$\begin{aligned}\sin\alpha_i^o &= \frac{y_i^o}{\left\|\mathbf{s}_i^o\right\|} = \frac{y_i}{\|\mathbf{s}_i\|} - \frac{1}{\|\mathbf{s}_i\|}(\mathbf{i}_y - \frac{y_i\mathbf{s}_i}{\|\mathbf{s}_i\|^2})\mathbf{n}_{si} \\ &= \sin\alpha_i - \frac{1}{\|\mathbf{s}_i\|}(\mathbf{i}_y - \frac{y_i\mathbf{s}_i}{\|\mathbf{s}_i\|^2})\mathbf{n}_{si},\ i = 1, 2, \cdots, M,\end{aligned} \tag{3.28}$$

where $\mathbf{i}_x = [1,\ 0],\ \mathbf{i}_y = [0,\ 1]$. Let $\mathbf{p}_{xi} = \mathbf{i}_x - \frac{x_i\mathbf{s}_i}{\|\mathbf{s}_i\|^2}$ denote the orthogonal projection matrix of $\frac{x_i}{\|\mathbf{s}_i\|}$ [44], and $\mathbf{p}_{yi} = \mathbf{i}_y - \frac{y_i\mathbf{s}_i}{\|\mathbf{s}_i\|^2}$ denote the orthogonal projection matrix of $\frac{y_i}{\|\mathbf{s}_i\|}$, we can get

$$\cos\alpha_1^o - \cos\alpha_i^o = \cos\alpha_1 - \cos\alpha_i + \frac{1}{\|\mathbf{s}_i\|}\mathbf{p}_{xi}\mathbf{n}_{si} - \frac{1}{\|\mathbf{s}_1\|}\mathbf{p}_{x1}\mathbf{n}_{s1} \tag{3.29}$$

and

$$\sin\alpha_1^o - \sin\alpha_i^o = \sin\alpha_1 - \sin\alpha_i + \frac{1}{\|\mathbf{s}_i\|}\mathbf{p}_{yi}\mathbf{n}_{si} - \frac{1}{\|\mathbf{s}_1\|}\mathbf{p}_{y1}\mathbf{n}_{s1} \tag{3.30}$$

Replacing the noise free components in (3.24) by their noisy expressions yields

$$\begin{aligned}&r_{i1} - n_{ri} - R_{i1} - \frac{\mathbf{s}_i^T}{\|\mathbf{s}_i\|}\mathbf{n}_{si} + \frac{\mathbf{s}_1^T}{\|\mathbf{s}_1\|}\mathbf{n}_{s1} \\ &= x^o(\cos\alpha_1 - \cos\alpha_i + \frac{1}{\|\mathbf{s}_i\|}\mathbf{p}_{xi}\mathbf{n}_{si} - \frac{1}{\|\mathbf{s}_1\|}\mathbf{p}_{x1}\mathbf{n}_{s1}) \\ &+ y^o(\sin\alpha_1 - \sin\alpha_i + \frac{1}{\|\mathbf{s}_i\|}\mathbf{p}_{yi}\mathbf{n}_{si} - \frac{1}{\|\mathbf{s}_1\|}\mathbf{p}_{y1}\mathbf{n}_{s1}),\ i = 2, 3, \cdots, M.\end{aligned} \tag{3.31}$$

Let e_i denote the noise term in (3.31),

$$\begin{aligned} e_i &= n_{ri} + \mathbf{v}_i \mathbf{n}_{si} - \mathbf{v}_1 \mathbf{n}_{s1} \\ &= x^o(\cos\alpha_1 - \cos\alpha_i) + y^o(\sin\alpha_1 - \sin\alpha_i), i = 2, 3, \cdots, M, \end{aligned} \tag{3.32}$$

where

$$\begin{aligned} \mathbf{v}_1 &= -(\frac{x^o}{\|\mathbf{s}_1\|}\mathbf{p}_{x1} + \frac{y^o}{\|\mathbf{s}_1\|}\mathbf{p}_{y1} - \frac{\mathbf{s}_1^T}{\|\mathbf{s}_1\|}) = -\Big[\frac{(\mathbf{u}^o - \mathbf{s}_1)^T}{\|\mathbf{s}_1\|} - \frac{(x^o x_1 + y^o y_1)\mathbf{s}_1^T}{\|\mathbf{s}_1\|^3}\Big] \\ \mathbf{v}_i &= \frac{x^o}{\|\mathbf{s}_i\|}\mathbf{p}_{xi} + \frac{y^o}{\|\mathbf{s}_i\|}\mathbf{p}_{yi} - \frac{\mathbf{s}_i^T}{\|\mathbf{s}_i\|} = \frac{(\mathbf{u}^o - \mathbf{s}_i)^T}{\|\mathbf{s}_i\|} - \frac{(x^o x_i + y^o y_i)\mathbf{s}_i^T}{\|\mathbf{s}_i\|^3}, i = 2, 3, \cdots, M. \end{aligned} \tag{3.33}$$

We can express (3.32) in the following matrix form

$$\mathbf{e} = \mathbf{h}_1 - \mathbf{G}_1 \boldsymbol{\theta}_1^o, \tag{3.34}$$

where $\mathbf{e} = [e_2, e_3, \cdots, e_M]^T$, $\boldsymbol{\theta}_1 = [x,\ y]^T$ and

$$\mathbf{h}_1 = \begin{bmatrix} r_{21} - R_{21} \\ \vdots \\ r_{M1} - R_{M1} \end{bmatrix}, \tag{3.35}$$

$$\mathbf{G}_1 = \begin{bmatrix} \cos\alpha_1 - \cos\alpha_2 & \sin\alpha_1 - \sin\alpha_2 \\ \vdots & \vdots \\ \cos\alpha_1 - \cos\alpha_M & \sin\alpha_1 - \sin\alpha_M \end{bmatrix} = \begin{bmatrix} \frac{x_1}{R_1} - \frac{x_2}{R_2} & \frac{y_1}{R_1} - \frac{y_2}{R_M} \\ \vdots & \vdots \\ \frac{x_1}{R_1} - \frac{x_M}{R_M} & \frac{y_1}{R_1} - \frac{y_M}{R_M} \end{bmatrix}. \tag{3.36}$$

From the definition of e_i in (3.32), we also have

$$\mathbf{e} = \mathbf{n}_r + \mathbf{V}\mathbf{n}_s, \tag{3.37}$$

where

$$\mathbf{V} = \begin{bmatrix} \mathbf{v}_1 & \mathbf{v}_2 & \mathbf{0} & \cdots & \mathbf{0} \\ \mathbf{v}_1 & \mathbf{0} & \mathbf{v}_3 & \cdots & \mathbf{0} \\ \vdots & \vdots & \vdots & \ddots & \vdots \\ \mathbf{v}_1 & \mathbf{0} & \mathbf{0} & \cdots & \mathbf{v}_M \end{bmatrix}. \tag{3.38}$$

The weighted LS solution is given by

$$\hat{\boldsymbol{\theta}}_1 = (\mathbf{G}_1^T \mathbf{W}_1 \mathbf{G}_1)^{-1} \mathbf{G}_1^T \mathbf{W}_1 \mathbf{h}_1, \tag{3.39}$$

where $\mathbf{W}_1 = E[\mathbf{e}\mathbf{e}^T]^{-1} = (\mathbf{Q}_r + \mathbf{V}\mathbf{Q}_s\mathbf{V}^T)^{-1}$ is the weighting matrix. If the sensor position error is small enough such that we ignore the noise in $\mathbf{G}_1$, the covariance matrix of $\boldsymbol{\theta}_1^o$ is

$$\text{cov}(\boldsymbol{\theta}_1^o) = (\mathbf{G}_1^T \mathbf{W}_1 \mathbf{G}_1)^{-1} \tag{3.40}$$

Since matrix $\mathbf{v}_i$ contains the true source location, $\mathbf{W}_1$ is not available in practice. To handle this situation, we shall begin by setting $\mathbf{W}_1$ to identity matrix $\mathbf{I}_{M-1}$ to get the initial guess for source location which is then used to construct $\mathbf{W}_1$. For most cases, found by simulations, the initial guess when ignoring the sensor position errors is sufficient enough to construct $\mathbf{W}_1$ and the performance degradation from this approximation is insignificant.

3.3.2 Performance Analysis

To get a better understanding about how the sensor position error affects the estimation accuracy of the source location, the source location CRLB in the presence of random sensor position errors is evaluated as following. Form data vector $\boldsymbol{\zeta} = [\mathbf{r}^T, \mathbf{s}^T]^T$, the Fisher information matrix (FIM) of the unknown $\boldsymbol{\lambda}^o = [\mathbf{u}^{oT}, \mathbf{s}^{oT}]^T$ is

$$\text{FIM} = -E\big[\frac{\partial^2 \ln p(\boldsymbol{\zeta}; \boldsymbol{\lambda}^o)}{\partial \boldsymbol{\lambda}^o \partial \boldsymbol{\lambda}^{oT}}\big] = \begin{bmatrix} \mathbf{X} & \mathbf{Y} \\ \mathbf{Y}^T & \mathbf{Z} \end{bmatrix}, \tag{3.41}$$

where $\ln p(\boldsymbol{\zeta}; \boldsymbol{\lambda}^o)$ is the logarithm of the probability density function of $\boldsymbol{\zeta}$ parameterized on $\boldsymbol{\lambda}^o$ and

$$\begin{aligned} \mathbf{X} &= -E\big[\frac{\partial^2 \ln p(\boldsymbol{\zeta}; \boldsymbol{\lambda}^o)}{\partial \mathbf{u}^o \partial \mathbf{u}^{oT}}\big] = \big(\frac{\partial \mathbf{r}^o}{\partial \mathbf{u}^o}\big)^T \mathbf{Q}_r^{-1} \big(\frac{\partial \mathbf{r}^o}{\partial \mathbf{u}^o}\big), \\ \mathbf{Y} &= -E\big[\frac{\partial^2 \ln p(\boldsymbol{\zeta}; \boldsymbol{\lambda}^o)}{\partial \mathbf{u}^o \partial \mathbf{s}^{oT}}\big] = \big(\frac{\partial \mathbf{r}^o}{\partial \mathbf{u}^o}\big)^T \mathbf{Q}_r^{-1} \big(\frac{\partial \mathbf{r}^o}{\partial \mathbf{s}^o}\big), \\ \mathbf{Z} &= -E\big[\frac{\partial^2 \ln p(\boldsymbol{\zeta}; \boldsymbol{\lambda}^o)}{\partial \mathbf{s}^o \partial \mathbf{s}^{oT}}\big] = \big(\frac{\partial \mathbf{r}^o}{\partial \mathbf{s}^o}\big)^T \mathbf{Q}_r^{-1} \big(\frac{\partial \mathbf{r}^o}{\partial \mathbf{s}^o}\big) + \mathbf{Q}_s^{-1}. \end{aligned} \tag{3.42}$$

The CRLB of the source location is given by

$$\begin{aligned} \text{CRLB}(\mathbf{u}^o) &= (\mathbf{X} - \mathbf{Y}\mathbf{Z}^{-1}\mathbf{Y}^T)^{-1} \\ &= \mathbf{X}^{-1} + \mathbf{X}^{-1}\mathbf{Y}(\mathbf{Z} - \mathbf{Y}^T\mathbf{X}^{-1}\mathbf{Y})^{-1}\mathbf{Y}^T\mathbf{X}^{-1}. \end{aligned} \tag{3.43}$$

The first term $\mathbf{X}^{-1}$ represents the source location CRLB without sensor location errors, and the second term corresponds to the increase of CRLB due to the sensor location errors. Rewriting $\mathbf{W}_1$ by applying the portend matrix inversion formula [47], we have

$$\mathbf{W}_1 = \mathbf{Q}_r^{-1} - \mathbf{Q}_r^{-1}\mathbf{V}(\mathbf{Q}_s^{-1} + \mathbf{V}^T\mathbf{Q}_r^{-1}\mathbf{V})\mathbf{V}^T\mathbf{Q}_r^{-1}. \tag{3.44}$$

Substituting (3.44) into (3.40) yields

$$\mathrm{cov}(\mathbf{u}^o)^{-1} = \mathbf{G}_1^T\mathbf{Q}_r^{-1}\mathbf{G}_1 - \mathbf{G}_1^T\mathbf{Q}_r^{-1}\mathbf{V}(\mathbf{Q}_s^{-1} + \mathbf{V}^T\mathbf{Q}_r^{-1}\mathbf{V})^{-1}\mathbf{V}^T\mathbf{Q}_r^{-T}\mathbf{G}_1. \tag{3.45}$$

Similarly, we can express CRLB($\mathbf{u}^o$) as

$$\mathrm{CRLB}(\mathbf{u}^o)^{-1} = \mathbf{A}^T\mathbf{Q}_r^{-1}\mathbf{A} - \mathbf{A}^T\mathbf{Q}_r^{-1}\mathbf{K}(\mathbf{Q}_s^{-1} + \mathbf{K}^T\mathbf{Q}_r^{-1}\mathbf{K})^{-1}\mathbf{K}^T\mathbf{Q}_r^{-T}\mathbf{A}, \tag{3.46}$$

where

$$\mathbf{A} = \frac{\partial \mathbf{r}^o}{\partial \mathbf{u}^o} = \begin{bmatrix} \frac{x_1-x^o}{r_1^o} - \frac{x_2-x^o}{r_2^o} - & \frac{y_1-y^o}{r_1^o} - - \frac{y_2-y^o}{r_2^o} \\ \vdots & \vdots \\ \frac{x_1-x^o}{r_1^o} - \frac{x_M-x^o}{r_2^o} & \frac{y_1-y^o}{r_1^o} - \frac{y_M-y^o}{r_M^o} \end{bmatrix}, \tag{3.47}$$

$$\mathbf{K} = \frac{\partial \mathbf{r}^o}{\partial \mathbf{s}^o} = \begin{bmatrix} \mathbf{k}_1 & \mathbf{k}_2 & \mathbf{0} & \cdots & \mathbf{0} \\ \mathbf{k}_1 & \mathbf{0} & \mathbf{k}_3 & \cdots & \mathbf{0} \\ \vdots & \vdots & \vdots & \ddots & \vdots \\ \mathbf{k}_1 & \mathbf{0} & \mathbf{0} & \cdots & \mathbf{k}_M \end{bmatrix}, \tag{3.48}$$

and

$$\mathbf{k}_1 = \frac{(\mathbf{u}^o - \mathbf{s}_1)^T}{\|\mathbf{s}_1\|}, \mathbf{k}_i = -\frac{(\mathbf{u}^o - \mathbf{s}_i)^T}{\|\mathbf{s}_i\|}, i = 2, 3, \cdots, M. \tag{3.49}$$

Condition 1. Large Equal Radius:

$$\frac{r^o}{R_i} = \frac{\|\mathbf{u}^o\|}{\|\mathbf{s}_i\|} \simeq 0.$$

Condition 2. The sensor position noise power σ_s^2 is very small.

When both Condition 1 and Condition 2 are satisfied, we have

$$\frac{(x^o x_i + y^o y_i)\mathbf{s}_i^T}{\|\mathbf{s}_i\|^3} = \frac{\|\mathbf{u}^o\|}{\|\mathbf{s}_i\|}\cos(\alpha_i - \alpha)\frac{\mathbf{s}_i^T}{\|\mathbf{s}_i\|} \simeq \mathbf{0}. \tag{3.50}$$

Therefore $\mathbf{v}_i \simeq -\mathbf{k}_i (i = 1, 2, \cdots, M)$ and $\mathbf{V} \simeq -\mathbf{K}$. In addition, $\mathbf{G}_1 \simeq \mathbf{A}$ in the LER conditions, thus $\text{CRLB}(\mathbf{u}^o)^{-1} \simeq \text{cov}(\mathbf{u}^o)^{-1}$, the proposed estimator can achieve optimum performance CRLB in the presence of sensor position errors.

Compared to the covariance matrix in the absence of sensor position errors, $\mathbf{V}$ is affected by the sensor position errors, therefore in the large noise levels, even though the covariance is dominant in MSE, the MSE will deviate from CRLB. That is why Condition 2 is required.

3.3.3 Simulations

In this section, we add sensor position errors to the simulation scenario in Table 3 in Section 3.2.3. The covariance matrix of the sensor position measurements is $\mathbf{Q}_s = \sigma_s^2 \mathbf{J}$, where $\mathbf{J} = diag[1, 1, 2, 2, 10, 10, 4, 4, 25, 25, 30, 30, 40, 40]$. σ_s^2 is the sensor position error power and it varies between 10^{-6} and 1. $\mathbf{Q}_r$ is the covariance matrix of the range measurement noise power $(c\sigma_r)^2$ that is fixed to 10^{-4}.

In the Figure 18, we show the MSEs of the proposed method, DMVLS and SCWLS when pretending sensor positions accurate. The gap between the MSEs and the CRLB becomes larger as σ_s^2 increases before σ_s^2 goes to $10^{-0.3}$. When the proposed method takes sensor position errors into account, its MSE can reach the CRLB when the sensor position error power is small.

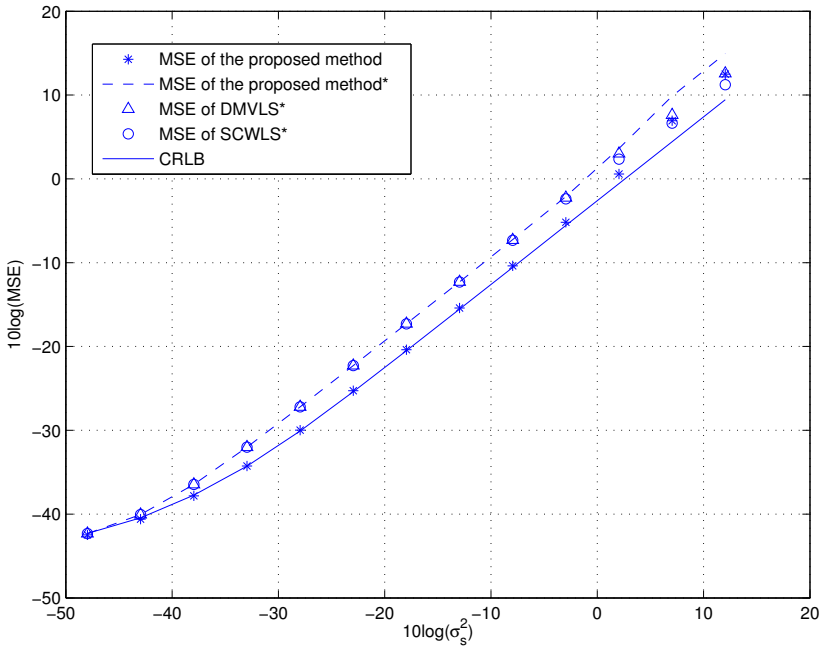

Figure 18: Performance comparison in the presence of sensor position errors with a certain 2D geometry. Star * marks the MSE when pretending sensor positions accurate.

3.4 Conclusion

We have presented a new method for the source localization under 2-D LER scenario. In the absence of sensor position errors, the theoretical analysis of the CRLB and MSE of the proposed method has been stated, and it is shown that the proposed estimator in 2-D is able to reach the CRLB in a wide range of TDOA measurement noise. The simulation results confirmed the theoretical development, and through the performance comparison with Chan-Ho, DMVLS and SCWLS, the proposed method is not only less time-consuming, but also more efficient in large TDOA measurement noise regions.

In the presence of sensor position errors under 2-D LER scenario, we took them

into account in the weighting matrix and addressed the theoretical CRLB analysis. The theory has shown the proposed estimator is able to reach CRLB in the LER scenario when the sensor position errors are small. In the simulations, the performance of the proposed estimator when considering sensor position errors confirmed the theoretical development. We have also shown the performance degradation of the proposed estimator, Chan-Ho, DMVLS and SCWLS when ignoring sensor position errors.

Chapter 4

Proposed Method in Three-dimensional Space

In this section, we will first illustrate the typical LER scenario in three dimensional space, followed by the development of the proposed method in 3-D based on TDOA measurements. We then analyze the theoretical performance of the proposed method and perform simulations to confirm the theoretical development. The performance of the proposed method in 3-D is also compared with Chan-Ho [18], SCWLS [45] and DMVLS [46] through simulations.

In the presence of sensor position error, we give the CRLB and MSE analysis following the steps in Section 3.3.2 and take the sensor position errors into consideration in the proposed estimator and eventually improve the source location estimation accuracy. Simulation result is presented to confirm the theoretical analysis.

4.1 LER Localization Scenario in 3-D

Consider one source and $M \geq 4$ sensors in a three-dimensional space as shown in Figure 19. Suppose sensors are located on or close to a sphere and the source is located at or near the center of this sphere. Let $\{*\}^o$ denote the noise-free quantity of $\{*\}$. The true source location $\mathbf{u}^o = [x^o,\ y^o,\ z^o]^T$ is unknown to be estimated using the TDOAs of the source signal received at the sensors. Let $\mathbf{s}_i^o = [x_i^o,\ y_i^o,\ z_i^o]^T$ be the true ith sensor position. The azimuth angles of the true source and the ith sensor locations with respect to the x-axis are denoted by α^o and α_i^o respectively, and the elevation angles of the true source and the ith sensor locations with respect to the x-y plane are denoted by β^o and β_i^o.

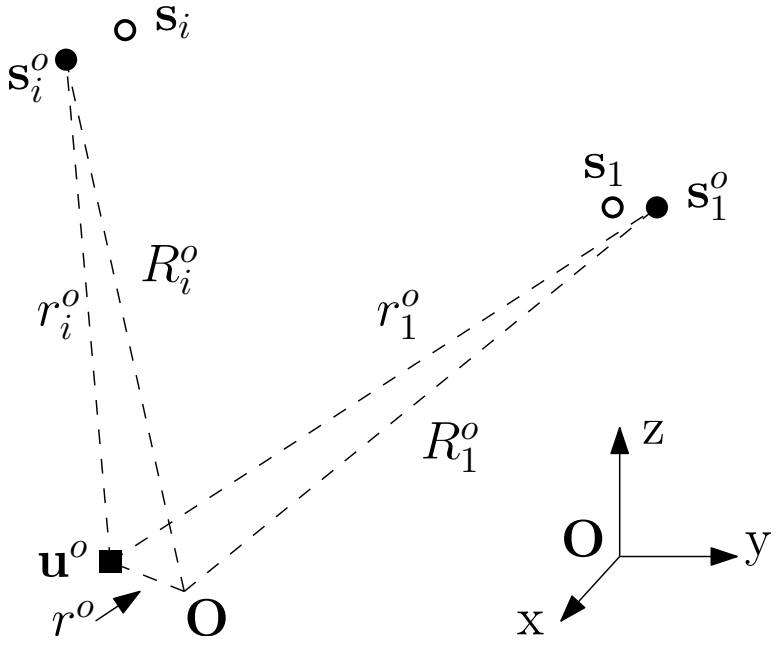

Figure 19: Illustration of the sensor geometry under 3-D LER conditions. Solid disks denote the unknown true sensor positions and open circles denote the available sensor positions that are erroneous.

The true range between the source and the ith sensor is

$$r_i^o = \|\mathbf{u}^o - \mathbf{s}_i^o\| = \sqrt{(x^o - x_i^o)^2 + (y^o - y_i^o)^2 + (z^o - z_i^o)^2}. \tag{4.1}$$

The distance between the origin $\mathbf{O}$ and the ith sensor is

$$R_i^o = \|\mathbf{s}_i^o\| = \sqrt{x_i^{o2} + y_i^{o2} + z_i^{o2}}. \tag{4.2}$$

And the distance between the origin $\mathbf{O}$ and the source, referred as the source range, is

$$r^o = \|\mathbf{u}^o\| = \sqrt{x^{o2} + y^{o2} + z^{o2}}. \tag{4.3}$$

The true range difference measurements from TDOAs, denoted by r_{i1}^o, are modeled as

$$\begin{aligned} r_{i1}^o &= r_i^o - r_1^o = c d_{i1}^o, \\ r_{i1}^o &= r_{i1} - n_{ri}, \ i = 2, 3, \cdots, M, \end{aligned} \tag{4.4}$$

where d_{i1}^o denote the true TDOA of a signal received by the sensor pair i and 1, c is the signal propagation speed, and n_{ri} is the range difference measurement noise. Collecting the TDOA measurements in the matrix form yields

$$\mathbf{r}^o = \mathbf{r} - \mathbf{n}_r, \tag{4.5}$$

where $\mathbf{r}^o = [r_{21}^o, r_{31}^o, \cdots, r_{M1}^o]^T$. The range difference measurement noise vector $\mathbf{n}_r = [n_{r2}, \cdots, n_{rM}]^T$ is assumed as a zero-mean Gaussian random vector, and has an $(M-1) \times (M-1)$ covariance matrix $\mathbf{Q}_r$.

In the absence of sensor position errors, we assume the available sensor locations $\mathbf{s}_i = [x_i,\ y_i,\ z_i]^T, i = 1, 2, \cdots, M$ are the same as the true sensor locations $\mathbf{s}_i^o$, so as the ith sensor range $R_i^o = R_i$.

In the presence of sensor position errors, the available sensor positions $\mathbf{s}_i$ are erroneous and the true sensor positions $\mathbf{s}_i^o$ are unknown. The available sensor positions can be modeled as

$$\mathbf{s}_i = \mathbf{s}_i^o + \mathbf{n}_{si} \tag{4.6}$$

where $\mathbf{n}_{si}$ represents the position error for sensor i and $\mathbf{n}_s = [\mathbf{n}_{s1}^T, \mathbf{n}_{s2}^T, \cdots, \mathbf{n}_{sM}^T]^T$ is also modeled as a zero-mean Gaussian random with covariance matrix $\mathbf{Q}_s$.

4.2 Closed-form Solution in the Absence of Sensor Position Errors

4.2.1 Algorithm Development

In the absence of sensor position error, we assume $\mathbf{s}_i = \mathbf{s}_i^o$ and $R_i^o = R_i$. According to the Law of Cosines, in the triangle formed by the origin, $\mathbf{u}^o$ and $\mathbf{s}_i$, we have

$$\begin{aligned} r_i^{o2} &= [R_i \cos\beta_i \cos(\alpha_i - \alpha^o) - r^o \cos\beta^o]^2 + [R_i \cos\beta_i \sin(\alpha_i - \alpha^o)]^2 \\ &\quad + (R_i \sin\beta_i - r^o \sin\beta^o)^2 \\ &= R_i^2 + r^{o2} - 2R_i r^o [\cos\beta_i \cos\beta^o \cos(\alpha_i - \alpha^o) + \sin\beta_i \sin\beta^o]. \end{aligned} \tag{4.7}$$

Using the Taylor series expansion, we can approximate r_i^o by

$$\begin{aligned} r_i^o &\simeq R_i[1 + \frac{r^{o2}}{2R_i^2} - \frac{r^o}{R_i}(\cos\beta_i \cos\beta^o \cos(\alpha_i - \alpha^o) + \sin\beta_i \sin\beta^o)] \\ &= R_i + \frac{r^{o2}}{2R_i} - r^o[\cos\beta_i \cos\beta^o \cos(\alpha_i - \alpha^o) + \sin\beta_i \sin\beta^o]. \end{aligned} \tag{4.8}$$

Then r_{i1}^o can be expressed as

$$\begin{aligned} r_{i1}^o &\simeq R_{i1} - r^o[\cos\beta_i \cos\beta^o \cos(\alpha_i - \alpha^o) + \sin\beta_i \sin\beta^o] \\ &\quad + r^o[\cos\beta_1 \cos\beta^o \cos(\alpha_1 - \alpha^o) + \sin\beta_1 \sin\beta^o] \\ &= R_{i1} + (r^o \cos\beta^o \cos\alpha^o)(\cos\beta_1 \cos\alpha_1 - \cos\beta_i \cos\alpha_i) \\ &\quad + (r^o \cos\beta^o \sin\alpha^o)(\cos\beta_1 \sin\alpha_1 - \cos\beta_i \sin\alpha_i) + (r^o \sin\beta^o)(\sin\beta_1 - \sin\beta_i), \end{aligned} \tag{4.9}$$

where $R_{i1} = R_i - R_1$ and $\frac{r^{o2}}{2}(\frac{1}{R_i} - \frac{1}{R_1}) \simeq 0$ when $R_i \gg r^o$. Let the source position estimate be $\boldsymbol{\theta} = [r\cos\beta\cos\alpha,\ r\cos\beta\sin\alpha,\ r\sin\beta]^T = [x,\ y,\ z]^T$. With noisy TDOA measurements, the equation error of (4.9) can be expressed in the matrix form as

$$\mathbf{n}_r = \mathbf{h} - \mathbf{G}\boldsymbol{\theta}^o, \tag{4.10}$$

where

$$\mathbf{G} = \begin{bmatrix} \cos\beta_1\cos\alpha_1 - \cos\beta_2\cos\alpha_2 & \cos\beta_1\sin\alpha_1 - \cos\beta_2\sin\alpha_2 & \sin\beta_1 - \sin\beta_2 \\ \vdots & \vdots & \vdots \\ \cos\beta_1\cos\alpha_1 - \cos\beta_M\cos\alpha_M & \cos\beta_1\sin\alpha_1 - \cos\beta_M\sin\alpha_M & \sin\beta_1 - \sin\beta_M \end{bmatrix}$$
$$= \begin{bmatrix} \frac{x_1}{R_1} - \frac{x_2}{R_2} & \frac{y_1}{R_1} - \frac{y_2}{R_2} & \frac{z_1}{R_1} - \frac{z_2}{R_2} \\ \vdots & \vdots & \vdots \\ \frac{x_1}{R_1} - \frac{x_M}{R_M} & \frac{y_1}{R_1} - \frac{y_M}{R_M} & \frac{z_1}{R_1} - \frac{z_M}{R_M} \end{bmatrix} \tag{4.11}$$

and

$$\mathbf{h} = \begin{bmatrix} r_{21} - R_{21} \\ \vdots \\ r_{M1} - R_{M1} \end{bmatrix}. \tag{4.12}$$

The weighted LS solution is

$$\hat{\boldsymbol{\theta}} = (\mathbf{G}^T\mathbf{W}\mathbf{G})^{-1}\mathbf{G}^T\mathbf{W}\mathbf{h}, \tag{4.13}$$

and the covariance matrix of $\boldsymbol{\theta}^o$ is

$$\mathrm{cov}(\boldsymbol{\theta}^o) = (\mathbf{G}^T\mathbf{W}\mathbf{G})^{-1}, \tag{4.14}$$

where $\mathbf{W} = \mathbf{Q}_r^{-1}$ is the weighting matrix.

The iterative method in section 3.2.1 is also applied to 3D cases due to the bias from the Taylor series expansion. The origin $\mathbf{O}$ is initialized as $(0, 0, 0)^T$. According to simulations with randomly distributed LER geometries, 5 iterations are enough

for the proposed method to converge in 3-D too.

4.2.2 Comparison With CRLB and Bias Analysis

As shown in section 3.2.2, to show the $\mathrm{cov}(\boldsymbol{\theta}^o)$ can achieve $\mathrm{CRLB}(\boldsymbol{\theta}^o)$ under the LER situations in 3D cases, we can prove that $\frac{\partial \mathbf{r}^o}{\partial \boldsymbol{\theta}^T}|_{\boldsymbol{\theta}\simeq\boldsymbol{\theta}^o} \simeq \mathbf{G}$. Here the partial derivative is found to be

$$\frac{\partial \mathbf{r}^o}{\partial \boldsymbol{\theta}^T}|_{\boldsymbol{\theta}=\boldsymbol{\theta}^o} = \begin{bmatrix} \frac{x_1-x^o}{r_1^o} - \frac{x_2-x^o}{r_2^o} & \frac{y_1-y^o}{r_1^o} - \frac{y_2-y^o}{r_2^o} & \frac{z_1-z^o}{r_1^o} - \frac{z_2-z^o}{r_2^o} \\ \vdots & \vdots & \vdots \\ \frac{x_1-x^o}{r_1^o} - \frac{x_M-x^o}{r_M^o} & \frac{y_1-y^o}{r_1^o} - \frac{y_M-y^o}{r_M^o} & \frac{z_1-z^o}{r_1^o} - \frac{z_M-z^o}{r_M^o} \end{bmatrix}. \tag{4.15}$$

In the 3-D LER conditions, $R_i \gg r^o$, $R_i \simeq r_i^o$

$$\frac{x^o}{r_i^o} \simeq \frac{x^o}{R_i} \leq \frac{r^o}{R_i} \simeq 0, \tag{4.16}$$

accordingly,

$$\frac{x_i}{R_i} \simeq \frac{x_i - x^o}{r_i^o}. \tag{4.17}$$

Similarly we have

$$\begin{aligned} \frac{y_i}{R_i} &\simeq \frac{y_i - y^o}{r_i^o}, \\ \frac{z_i}{R_i} &\simeq \frac{z_i - z^o}{r_i^o}. \end{aligned} \tag{4.18}$$

Therefore

$$\mathbf{G} \simeq \left.\frac{\partial \mathbf{r}^o}{\partial \boldsymbol{\theta}^T}\right|_{\boldsymbol{\theta}=\boldsymbol{\theta}^o}, \tag{4.19}$$

the proposed estimator is able to achieve the optimum performance CRLB when LER is sufficiently satisfied in 3-D.

The proposed estimator is biased due to the inaccuracy of Taylor series expansion. $\Delta\{*\}$ is used to denote the noise component in $\{*\}$. Upon substituting $\mathbf{G} = \mathbf{G}^o$, $\mathbf{h} = \mathbf{n}_r + \mathbf{h}^o$ and $\boldsymbol{\theta} = \Delta\boldsymbol{\theta} + \boldsymbol{\theta}^o$ to (4.13), we have

$$\Delta\boldsymbol{\theta} = (\mathbf{G}^T\mathbf{W}\mathbf{G})^{-1}\mathbf{G}^T\mathbf{W}(\mathbf{n}_r + \mathbf{h}^o - \mathbf{G}\boldsymbol{\theta}^o). \tag{4.20}$$

Let $\mathbf{b} = (\mathbf{G}^T\mathbf{W}\mathbf{G})^{-1}\mathbf{G}^T\mathbf{W}(\mathbf{h}^o - \mathbf{G}\boldsymbol{\theta}^o)$ denote the bias component. Then the MSE($\boldsymbol{\theta}$) can be expressed by

$$\text{MSE}(\boldsymbol{\theta}) = E[\Delta\boldsymbol{\theta}^T\Delta\boldsymbol{\theta}] = \text{cov}(\boldsymbol{\theta}^o) + \mathbf{b}^T\mathbf{b}. \tag{4.21}$$

In sufficient LER localization scenario where sensor range R_i is much greater than the source range r, the value of the bias component from the Taylor series expansion can be ignorable. But when the range ratio is not large enough and the TDOA measurement noise power is small, the bias term is dominant in MSE. In this case, iterations are applied to update the origin and create a sufficient LER scenario with larger range ratios, and the solutions will converge to a location estimate whose accuracy can reach the CRLB. In relatively large noise regions, the covariance is dominate and the bias becomes ignorable. However, when the noise is large, the solutions from iterations may not converge at all. Through step (a) in the iteration procedure, we can check the divergence and stop iterations before the solution diverges. Since the observation matrix $\mathbf{G}$ is independent from TDOA measurement noises, the proposed estimator can reach the CRLB in large noise regions before divergence.

4.2.3 Simulations

In the LER conditions, sensors form a uniform or close to uniform circular array, and $R_i \simeq R,\ i = 1, 2, \cdots, M$. We define $\frac{R}{r^o}$ as the sensor range and the source range ratio (hereafter called range ratio).

Similarly we present the bias reduction trend of the proposed method without iterations when the range ratio increases in three dimensional space. Consider a uniform circular array with 7 sensors and the source is fixed close to the circular array center with the source range equal to 1. The sensor range ratios vary among the given values $[5, 20, 50, 100, 300, 500, 1000]$. The sensors' azimuth angles with respect to the x-axis are fixed as $[223°, 232°, 118°, 55°, 66°, 164°, 192°]$, and the elevation angles with respect to the x-y plane are fixed as $[33°, 145°, 281°, 95°, 111°, 66°, 272°]$. The azimuth and elevation angles for the source are both $10°$. σ_r^2 is the TDOA measurement error power and $(c\sigma_r)^2$ is fixed as 10^{-7}.

In Figure 20, we compare the simulation MSE, the theoretical MSE, covariance and CRLB. Bias corresponds to the difference between the theoretical MSE and the covariance. With the range ratio increasing, the accuracy of Taylor series expansion also improves which reduces the bias value. On the other hand, if we set $(c\sigma_r)^2$ to vary between 10^{-7} and 10^4 and fix range ratio to be 20, as shown in Figure 21, the bias component can be dominant in small noise regions, but ignorable in large noise regions.

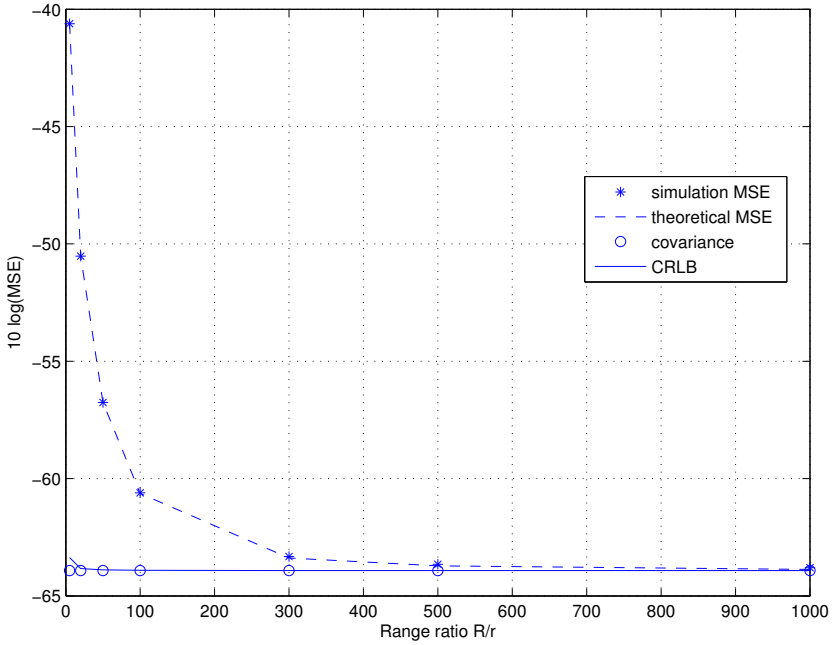

Figure 20: The bias and MSE behaviors of the proposed method in 3-D with $(c\sigma_r)^2 = 10^{-7}$

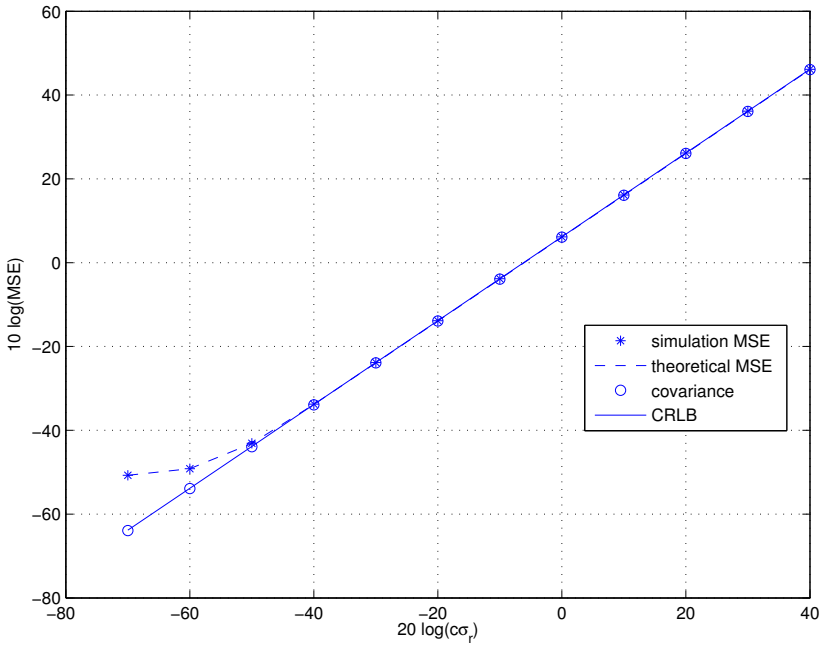

Figure 21: The bias and MSE behaviors of the proposed method in a certain 3-D geometry with the range ratio equal to 20

Next we present two simulation examples to assess the relative performance of the proposed method, DMVLS, SCWLS and Chan-Ho method. The performance measure is the Mean Square Error as a function of noise powers $(c\sigma_r)^2$. In the simulations, DMVLS is initialized with the true source location. Its root selection strategy is to choose the root that minimizes the cost function (2.63) in section 2.4.3.

Example 4.1. Sensors are randomly distributed along a uniform circle and sensor ranges are fixed to be 40. We assume there are small randomly distributed fluctuations of sensor ranges between 0 and 1. The source has a randomly distributed range between 0 and 10. The azimuth and elevation angles of the source and the sensors are randomly distributed between 0° and 360°. We perform 100 randomly distributed geometries and 1000 ensemble runs for each geometry.

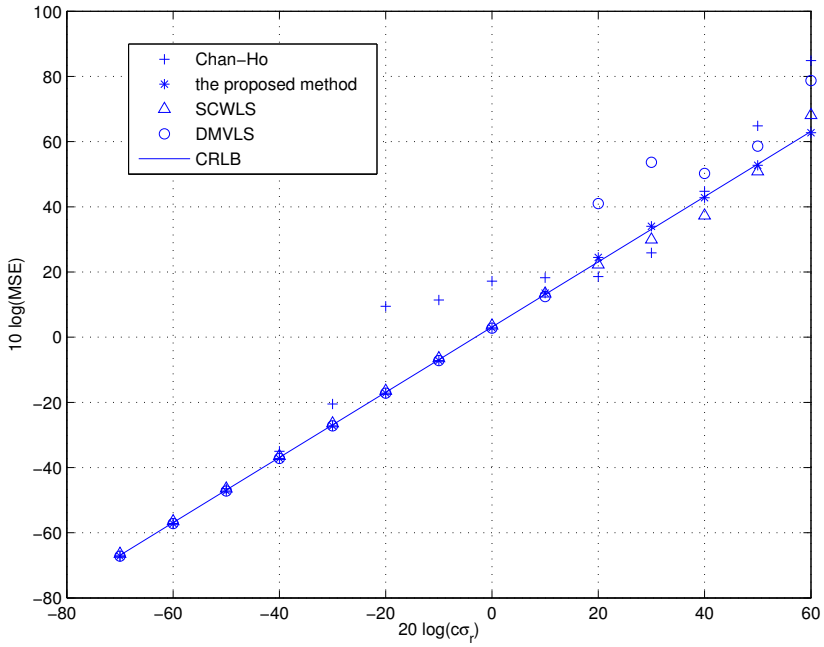

Figure 22: Performance comparison with randomly distributed 3D geometries

Figure 22 shows the performance comparison of the proposed method, DMVLS, SCWLS and Chan-Ho method with randomly distributed 3-D geometries. In this figure, the proposed method is able to reach the CRLB in the whole given noise regions. Chan-Ho method can reach CRLB in the small noise regions and it has a threshold effect when noise power $(c\sigma_r)^2$ goes to 10^{-3}. The MSEs of DMVLS and SCWLS start to deviate from the CRLB when the noise power gets larger than 10^2. Compared with DMVLS, the MSE of SCWLS has smaller deviations from the bound.

Table 4 shows the averaged computation time comparison for each ensemble run in 3-D randomly distributed geometries. The proposed method in 3-D is much more time efficient compared to DMVLS and SCWLS.

Table 4: Comparison of the averaged computation time for each ensemble run in 3-D randomly distributed geometries

Algorithm	The Proposed Method	Chan-Ho	DMVLS	SCWLS
Computation Time (second)	4.66×10^{-4}	3.07×10^{-4}	1.08×10^{-3}	1.99×10^{-3}

Example 4.2. In this example, we show the estimate accuracy comparison from a certain 3-D LER geometry. The geometry is shown in Table 5. 2000 ensemble runs are performed.

Table 5: Geometry information of a certain 3-D LER scenario

Geometry	Range	Azimuth Angle	Elevation Angle
Ture Source Location	0.4	24°	50°
Available Source Locations	4	17°	238°
		282°	46°
		86°	290°
		268°	77°
		61°	300°
		156°	304°
		29°	344°

In the Figure 23, Chan-Ho method fails due to the ill-conditioned measurement matrix and its performance is affected seriously by the TDOA measurement noises. DMVLS and SCWLS deviate from the CRLB when noise power is larger than 1. The proposed method can reach the CRLB in the whole given noise regions besides a 1.5dB deviation from the CRLB when the noise power is 1. In this case, affected by the TDOA noises, the solution may converge towards a location whose accuracy is a little worse than the CRLB, which causes the slight deviation.

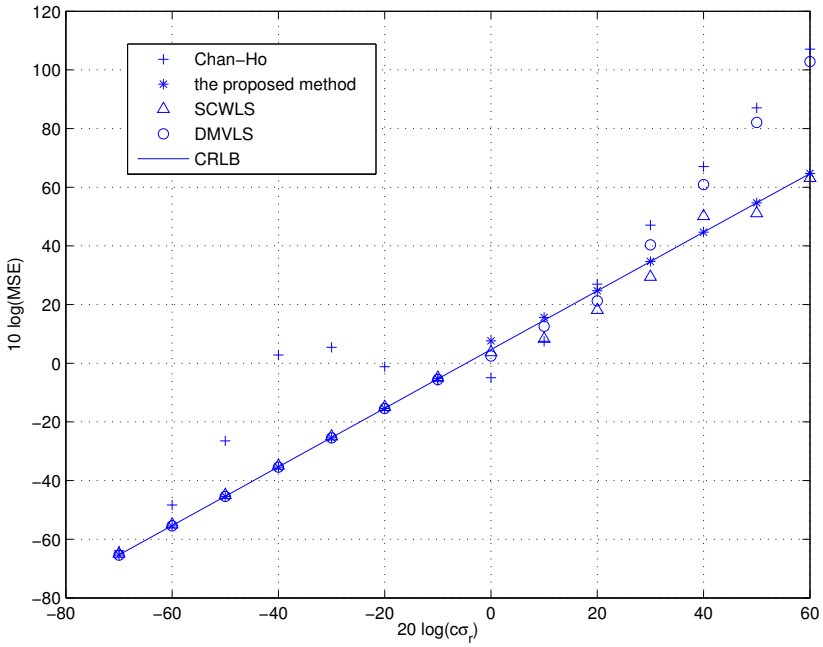

Figure 23: Performance comparison with a certain 3D geometry

4.3 Closed-form Solutions with Sensor Position Errors

4.3.1 Algorithm Development

We can follow the procedures in Section 3.3.1 to take sensor position errors into account. Rewriting (4.9) into a noiseless form gives

$$\begin{aligned} r_{i1}^o - R_{i1}^o = &(r^o \cos\beta^o \cos\alpha^o)(\cos\beta_1^o \cos\alpha_1^o - \cos\beta_i^o \cos\alpha_i^o) \\ &+ (r^o \cos\beta^o \sin\alpha^o)(\cos\beta_1^o \sin\alpha_1^o - \cos\beta_i^o \sin\alpha_i^o) \\ &+ (r^o \sin\beta^o)(\sin\beta_1^o - \sin\beta_i^o),\ \ i = 2, 3, \cdots, M. \end{aligned} \tag{4.22}$$

From the mathematics in section 3.3.1, we have the true sensor range difference $R_{i1}^o = R_{i1} - \frac{\mathbf{s}_i^T}{\|\mathbf{s}_i\|}\mathbf{n}_{si} + \frac{\mathbf{s}_1^T}{\|\mathbf{s}_1\|}\mathbf{n}_{s1}, i = 2, 3, \cdots, M$. Similarly,

$$\begin{aligned}\cos\beta_i^o \cos\alpha_i^o &= \frac{x_i^o}{\left\|\mathbf{s}_i^o\right\|} = \frac{x_i}{\|\mathbf{s}_i\|} - \frac{1}{\|\mathbf{s}_i\|}(\mathbf{i}_x - \frac{x_i\mathbf{s}_i}{\|\mathbf{s}_i\|^2})\mathbf{n}_{si} \\ &= \cos\beta_i\cos\alpha_i - \frac{1}{\|\mathbf{s}_i\|}(\mathbf{i}_x - \frac{x_i\mathbf{s}_i}{\|\mathbf{s}_i\|^2})\mathbf{n}_{si},\ i = 1, 2, \cdots, M,\end{aligned} \tag{4.23}$$

$$\begin{aligned}\cos\beta_i^o \sin\alpha_i^o &= \frac{y_i^o}{\left\|\mathbf{s}_i^o\right\|} = \frac{y_i}{\|\mathbf{s}_i\|} - \frac{1}{\|\mathbf{s}_i\|}(\mathbf{i}_y - \frac{y_i\mathbf{s}_i}{\|\mathbf{s}_i\|^2})\mathbf{n}_{si} \\ &= \cos\beta_i\sin\alpha_i - \frac{1}{\|\mathbf{s}_i\|}(\mathbf{i}_y - \frac{y_i\mathbf{s}_i}{\|\mathbf{s}_i\|^2})\mathbf{n}_{si},\ i = 1, 2, \cdots, M,\end{aligned} \tag{4.24}$$

$$\begin{aligned}\sin\beta_i^o &= \frac{z_i^o}{\left\|\mathbf{s}_i^o\right\|} = \frac{z_i}{\|\mathbf{s}_i\|} - \frac{1}{\|\mathbf{s}_i\|}(\mathbf{i}_z - \frac{z_i\mathbf{s}_i}{\|\mathbf{s}_i\|^2})\mathbf{n}_{si} \\ &= \sin\beta_i - \frac{1}{\|\mathbf{s}_i\|}(\mathbf{i}_z - \frac{z_i\mathbf{s}_i}{\|\mathbf{s}_i\|^2})\mathbf{n}_{si},\ i = 1, 2, \cdots, M,\end{aligned} \tag{4.25}$$

where $\mathbf{i}_x = [1, 0, 0],\ \mathbf{i}_y = [0, 1, 0],\ \mathbf{i}_z = [0, 0, 1]$.

Let $\mathbf{p}_{xi} = \mathbf{i}_x - \frac{x_i\mathbf{s}_i}{\|\mathbf{s}_i\|^2}$, $\mathbf{p}_{yi} = \mathbf{i}_y - \frac{y_i\mathbf{s}_i}{\|\mathbf{s}_i\|^2}$, $\mathbf{p}_{zi} = \mathbf{i}_z - \frac{z_i\mathbf{s}_i}{\|\mathbf{s}_i\|^2}$ denote the orthogonal projection matrix of $\frac{x_i}{\|\mathbf{s}_i\|}$, $\frac{y_i}{\|\mathbf{s}_i\|}$, $\frac{z_i}{\|\mathbf{s}_i\|}$ respectively, we can get

$$\begin{aligned}&\cos\beta_1^o\cos\alpha_1^o - \cos\beta_i^o\cos\alpha_i^o \\ &= \cos\beta_1\cos\alpha_1 - \cos\beta_i\cos\alpha_i + \frac{1}{\|\mathbf{s}_i\|}\mathbf{p}_{xi}\mathbf{n}_{si} - \frac{1}{\|\mathbf{s}_1\|}\mathbf{p}_{x1}\mathbf{n}_{s1},\end{aligned} \tag{4.26}$$

$$\begin{aligned}&\cos\beta_1^o\sin\alpha_1^o - \cos\beta_i^o\sin\alpha_i^o \\ &= \cos\beta_1\sin\alpha_1 - \cos\beta_i\sin\alpha_i + \frac{1}{\|\mathbf{s}_i\|}\mathbf{p}_{yi}\mathbf{n}_{si} - \frac{1}{\|\mathbf{s}_1\|}\mathbf{p}_{y1}\mathbf{n}_{s1},\end{aligned} \tag{4.27}$$

$$\sin\beta_1^o - \sin\beta_i^o = \sin\beta_1 - \sin\beta_i + \frac{1}{\|\mathbf{s}_i\|}\mathbf{p}_{zi}\mathbf{n}_{si} - \frac{1}{\|\mathbf{s}_1\|}\mathbf{p}_{z1}\mathbf{n}_{s1}, \tag{4.28}$$

where $i = 2, 3, \cdots, M$. Replacing the noise free components in (4.22) by their noisy

expressions yields

$$
\begin{aligned}
& r_{i1} - n_{ri} - R_{i1} - \frac{\mathbf{s}_i^T}{\|\mathbf{s}_i\|}\mathbf{n}_{si} + \frac{\mathbf{s}_1^T}{\|\mathbf{s}_1\|}\mathbf{n}_{s1} \\
& = (r^o \cos\beta^o \cos\alpha^o)(\cos\beta_1 \cos\alpha_1 - \cos\beta_i \cos\alpha_i + \frac{1}{\|\mathbf{s}_i\|}\mathbf{p}_{xi}\mathbf{n}_{si} - \frac{1}{\|\mathbf{s}_1\|}\mathbf{p}_{x1}\mathbf{n}_{s1}) \\
& + (r^o \cos\beta^o \sin\alpha^o)(\cos\beta_1 \sin\alpha_1 - \cos\beta_i \sin\alpha_i + \frac{1}{\|\mathbf{s}_i\|}\mathbf{p}_{yi}\mathbf{n}_{si} - \frac{1}{\|\mathbf{s}_1\|}\mathbf{p}_{y1}\mathbf{n}_{s1}) \\
& + (r^o \sin\beta^o)(\sin\beta_1 - \sin\beta_i + \frac{1}{\|\mathbf{s}_i\|}\mathbf{p}_{zi}\mathbf{n}_{si} - \frac{1}{\|\mathbf{s}_1\|}\mathbf{p}_{z1}\mathbf{n}_{s1}), i = 2, 3, \cdots, M.
\end{aligned}
\tag{4.29}
$$

Let e_i denote the noise term in (4.29),

$$
\begin{aligned}
e_i &= n_{ri} + \mathbf{v}_i\mathbf{n}_{si} - \mathbf{v}_1\mathbf{n}_{s1} \\
&= (r^o \cos\beta^o \cos\alpha^o)(\cos\beta_1 \cos\alpha_1 - \cos\beta_i \cos\alpha_i) \\
&\quad + (r^o \cos\beta^o \sin\alpha^o)(\cos\beta_1 \sin\alpha_1 - \cos\beta_i \sin\alpha_i) + (r^o \sin\beta^o)(\sin\beta_1 - \sin\beta_i),
\end{aligned}
\tag{4.30}
$$

where

$$
\begin{aligned}
\mathbf{v}_1 &= -(\frac{x^o}{\|\mathbf{s}_1\|}\mathbf{p}_{x1} + \frac{y^o}{\|\mathbf{s}_1\|}\mathbf{p}_{y1} + \frac{z^o}{\|\mathbf{s}_1\|}\mathbf{p}_{z1} - \frac{\mathbf{s}_1^T}{\|\mathbf{s}_1\|}) \\
&= -\big[\frac{(\mathbf{u}^o - \mathbf{s}_1)^T}{\|\mathbf{s}_1\|} - \frac{(x^o x_1 + y^o y_1 + z^o z_1)\mathbf{s}_1^T}{\|\mathbf{s}_1\|^3}\big], \\
\mathbf{v}_i &= \frac{x^o}{\|\mathbf{s}_i\|}\mathbf{p}_{xi} + \frac{y^o}{\|\mathbf{s}_i\|}\mathbf{p}_{yi} + \frac{z^o}{\|\mathbf{s}_1\|}\mathbf{p}_{z1} - \frac{\mathbf{s}_i^T}{\|\mathbf{s}_i\|} \\
&= \frac{(\mathbf{u}^o - \mathbf{s}_i)^T}{\|\mathbf{s}_i\|} - \frac{(x^o x_1 + y^o y_1 + z^o z_1)\mathbf{s}_i^T}{\|\mathbf{s}_i\|^3}, i = 2, 3, \cdots, M.
\end{aligned}
\tag{4.31}
$$

We can express (4.30) in the following matrix form

$$
\mathbf{e} = \mathbf{h}_1 - \mathbf{G}_1\boldsymbol{\theta}_1^o, \tag{4.32}
$$

where $\mathbf{e} = [e_2, e_3, \cdots, e_M]^T$,

$$\mathbf{G} = \begin{bmatrix} \cos\beta_1\cos\alpha_1 - \cos\beta_2\cos\alpha_2 & \cos\beta_1\sin\alpha_1 - \cos\beta_2\sin\alpha_2 & \sin\beta_1 - \sin\beta_2 \\ \vdots & \vdots & \vdots \\ \cos\beta_1\cos\alpha_1 - \cos\beta_M\cos\alpha_M & \cos\beta_1\sin\alpha_1 - \cos\beta_M\sin\alpha_M & \sin\beta_1 - \sin\beta_M \end{bmatrix}$$
$$= \begin{bmatrix} \frac{x_1}{R_1} - \frac{x_2}{R_2} & \frac{y_1}{R_1} - \frac{y_2}{R_2} & \frac{z_1}{R_1} - \frac{z_2}{R_2} \\ \vdots & \vdots & \vdots \\ \frac{x_1}{R_1} - \frac{x_M}{R_M} & \frac{y_1}{R_1} - \frac{y_M}{R_M} & \frac{z_1}{R_1} - \frac{z_M}{R_M} \end{bmatrix}, \tag{4.33}$$

$$\mathbf{h} = \begin{bmatrix} r_{21} - R_{21} \\ \vdots \\ r_{M1} - R_{M1} \end{bmatrix}, \quad \boldsymbol{\theta}_1 = \begin{bmatrix} r\cos\beta\cos\alpha \\ r\cos\beta\sin\alpha \\ r\sin\beta \end{bmatrix} = \begin{bmatrix} x \\ y \\ z \end{bmatrix}. \tag{4.34}$$

From the definition of e_i in (4.30), we also have

$$\mathbf{e} = \mathbf{n}_r + \mathbf{V}\mathbf{n}_s, \tag{4.35}$$

where

$$\mathbf{V} = \begin{bmatrix} \mathbf{v}_1 & \mathbf{v}_2 & \mathbf{0} & \cdots & \mathbf{0} \\ \mathbf{v}_1 & \mathbf{0} & \mathbf{v}_3 & \cdots & \mathbf{0} \\ \vdots & \vdots & \vdots & \ddots & \vdots \\ \mathbf{v}_1 & \mathbf{0} & \mathbf{0} & \cdots & \mathbf{v}_M \end{bmatrix}. \tag{4.36}$$

The weighted LS solution is given by

$$\hat{\boldsymbol{\theta}}_1 = (\mathbf{G}_1^T\mathbf{W}_1\mathbf{G}_1)^{-1}\mathbf{G}_1^T\mathbf{W}_1\mathbf{h}_1, \tag{4.37}$$

where $\mathbf{W}_1 = E[\mathbf{e}\mathbf{e}^T]^{-1} = (\mathbf{Q}_r + \mathbf{V}\mathbf{Q}_s\mathbf{V}^T)^{-1}$ is the weighting matrix. If the sensor position error is small enough such that we ignore the noise in $\mathbf{G}_1$, the covariance matrix of $\boldsymbol{\theta}_1$ is

$$\text{cov}(\boldsymbol{\theta}_1^o) = (\mathbf{G}_1^T\mathbf{W}_1\mathbf{G}_1)^{-1}. \tag{4.38}$$

Since matrix $\mathbf{v}_i$ contains the true source location, $\mathbf{W}_1$ is not available in practice. To handle this situation, we shall begin by setting $\mathbf{W}_1$ to identity matrix $\mathbf{I}_{M-1}$ to get the initial guess for source location which is then used to construct $\mathbf{W}_1$. For most cases, found by simulations, the initial guess when ignoring the sensor position errors is sufficient enough to construct $\mathbf{W}_1$ and the performance degradation from this approximation is insignificant.

4.3.2 Performance Analysis

From section 3.3.2, we already have a good understanding about how to evaluate the source location CRLB in the presence of randomly distributed sensor position errors and about the sensor position error affects the estimation accuracy of the source location, the source location CRLB in the presence of random sensor position errors is evaluated as following. Form data vector $\boldsymbol{\zeta} = [\mathbf{r}^T, \mathbf{s}^T]^T$, the Fisher information matrix (FIM) of the unknown $\boldsymbol{\lambda} = [\mathbf{u}^{oT}, \mathbf{s}^{oT}]$ is

$$\text{FIM} = -E\big[\frac{\partial^2 \ln p(\boldsymbol{\zeta};\boldsymbol{\lambda}^o)}{\partial\boldsymbol{\lambda}^o\partial\boldsymbol{\lambda}^{oT}}\big] = \begin{bmatrix} \mathbf{X} & \mathbf{Y} \\ \mathbf{Y}^T & \mathbf{Z} \end{bmatrix}, \tag{4.39}$$

where $\ln p(\boldsymbol{\zeta};\boldsymbol{\lambda}^o)$ is the logarithm of the probability density function of $\boldsymbol{\zeta}$ parameterized on $\boldsymbol{\lambda}^o$ and

$$\begin{aligned}
\mathbf{X} &= -E\big[\frac{\partial^2 \ln p(\boldsymbol{\zeta};\boldsymbol{\lambda}^o)}{\partial \mathbf{u}^o \partial \mathbf{u}^{oT}}\big] = \big(\frac{\partial \mathbf{r}^o}{\partial \mathbf{u}^o}\big)^T \mathbf{Q}_r^{-1} \big(\frac{\partial \mathbf{r}^o}{\partial \mathbf{u}^o}\big), \\
\mathbf{Y} &= -E\big[\frac{\partial^2 \ln p(\boldsymbol{\zeta};\boldsymbol{\lambda}^o)}{\partial \mathbf{u}^o \partial \mathbf{s}^{oT}}\big] = \big(\frac{\partial \mathbf{r}^o}{\partial \mathbf{u}^o}\big)^T \mathbf{Q}_r^{-1} \big(\frac{\partial \mathbf{r}^o}{\partial \mathbf{s}^o}\big), \\
\mathbf{Z} &= -E\big[\frac{\partial^2 \ln p(\boldsymbol{\zeta};\boldsymbol{\lambda}^o)}{\partial \mathbf{s}^o \partial \mathbf{s}^{oT}}\big] = \big(\frac{\partial \mathbf{r}^o}{\partial \mathbf{s}^o}\big)^T \mathbf{Q}_r^{-1} \big(\frac{\partial \mathbf{r}^o}{\partial \mathbf{s}^o}\big) + \mathbf{Q}_s^{-1}.
\end{aligned} \tag{4.40}$$

The CRLB of the source location is given by

$$\begin{aligned}
\mathrm{CRLB}(\mathbf{u}^o) &= (\mathbf{X} - \mathbf{Y}\mathbf{Z}^{-1}\mathbf{Y}^T)^{-1} \\
&= \mathbf{X}^{-1} + \mathbf{X}^{-1}\mathbf{Y}(\mathbf{Z} - \mathbf{Y}^T\mathbf{X}^{-1}\mathbf{Y})^{-1}\mathbf{Y}^T\mathbf{X}^{-1}.
\end{aligned} \tag{4.41}$$

The first term $\mathbf{X}^{-1}$ represents the source location CRLB without sensor location errors, and the second term corresponds to the increase of CRLB due to the sensor location errors. Rewriting $\mathbf{W}_1$ by applying the portend matrix inversion formula, we have

$$\mathbf{W}_1 = \mathbf{Q}_r^{-1} - \mathbf{Q}_r^{-1}\mathbf{V}(\mathbf{Q}_s^{-1} + \mathbf{V}^T\mathbf{Q}_r^{-1}\mathbf{V})\mathbf{V}^T\mathbf{Q}_r^{-1}. \tag{4.42}$$

Substituting (4.42) into (4.38) yields

$$\mathrm{cov}(\mathbf{u}^o)^{-1} = \mathbf{G}_1^T\mathbf{Q}_r^{-1}\mathbf{G}_1 - \mathbf{G}_1^T\mathbf{Q}_r^{-1}\mathbf{V}(\mathbf{Q}_s^{-1} + \mathbf{V}^T\mathbf{Q}_r^{-1}\mathbf{V})^{-1}\mathbf{V}^T\mathbf{Q}_r^{-T}\mathbf{G}_1. \tag{4.43}$$

Similarly, we can express $\mathrm{CRLB}(\mathbf{u}^o)$ as

$$\mathrm{CRLB}(\mathbf{u}^o)^{-1} = \boldsymbol{A}^T\mathbf{Q}_r^{-1}\mathbf{A} - \mathbf{A}^T\mathbf{Q}_r^{-1}\mathbf{K}(\mathbf{Q}_s^{-1} + \mathbf{K}^T\mathbf{Q}_r^{-1}\mathbf{K})^{-1}\mathbf{K}^T\mathbf{Q}_r^{-T}\mathbf{A}, \tag{4.44}$$

where

$$\mathbf{A} = \frac{\partial \mathbf{r}^o}{\partial \mathbf{u}^o} = \begin{bmatrix} \frac{x_1 - x^o}{r_1^o} - \frac{x_2 - x^o}{r_2^o} & \frac{y_1 - y^o}{r_1^o} - \frac{y_2 - y^o}{r_2^o} & \frac{z_1 - z^o}{r_1^o} - \frac{z_2 - z^o}{r_2^o} \\ \vdots & \vdots & \vdots \\ \frac{x_1 - x^o}{r_1^o} - \frac{x_M - x^o}{r_M^o} & \frac{y_1 - y^o}{r_1^o} - \frac{y_M - y^o}{r_M^o} & \frac{z_1 - z^o}{r_1^o} - \frac{z_M - z^o}{r_M^o} \end{bmatrix}, \tag{4.45}$$

$$\mathbf{K} = \frac{\partial \mathbf{r}^o}{\partial \mathbf{s}^o} = \begin{bmatrix} \mathbf{k}_1 & \mathbf{k}_2 & \mathbf{0} & \cdots & \mathbf{0} \\ \mathbf{k}_1 & \mathbf{0} & \mathbf{k}_3 & \cdots & \mathbf{0} \\ \vdots & \vdots & \vdots & \ddots & \vdots \\ \mathbf{k}_1 & \mathbf{0} & \mathbf{0} & \cdots & \mathbf{k}_M \end{bmatrix}, \tag{4.46}$$

$$\mathbf{k}_1 = \frac{(\mathbf{u}^o - \mathbf{s}_1)^T}{\|\mathbf{s}_1\|},\ \mathbf{k}_i = -\frac{(\mathbf{u}^o - \mathbf{s}_i)^T}{\|\mathbf{s}_i\|}, i = 2, 3, \cdots, M. \tag{4.47}$$

Condition 1 and Condition 2 in Section 3.3.2 can also be applied to 3-D. When they are both satisfied, we have

$$\frac{(x^o x_i + y^o y_i + z^o z_i)\mathbf{s}_i^T}{\|\mathbf{s}_i\|^3} = \frac{\|\mathbf{u}^o\|}{\|\mathbf{s}_i\|}\cos(\phi_i)\frac{\mathbf{s}_i^T}{\|\mathbf{s}_i\|} \simeq \mathbf{0}, i = 1, 2, \cdots, M, \tag{4.48}$$

where $cos(\phi_i) = \cos\beta_i \cos\beta^o \cos(\alpha_i - \alpha^o) + \sin\beta_i \sin\beta^o$ according to Equation (4.7). Therefore $\mathbf{v}_i \simeq -\mathbf{k}_i (i = 1, 2, \cdots, M)$ and $\mathbf{V} \simeq -\mathbf{K}$. In addition, $\mathbf{G}_1 \simeq \mathbf{A}$ in the LER conditions, thus $\text{CRLB}(\mathbf{u}^o)^{-1} \simeq \text{cov}(\mathbf{u}^o)^{-1}$, the proposed estimator can achieve optimum performance CRLB in the presence of sensor position errors.

4.3.3 Simulations

In this section, we add sensor position errors to the simulation scenario in Table 5 in Section 4.2.3. The covariance matrix of the sensor position measurements is $\mathbf{Q}_s =$

$\sigma_s^2\mathbf{J}$, where $\mathbf{J} = diag[1,1,1,2,2,2,10,10,10,4,4,4,25,25,25,30,30,30,40,40,40]$. σ_s^2 is the sensor position error power and it varies between 10^{-6} and 1. $\mathbf{Q}_r = \sigma_r^2$ is the covariance matrix of the range measurement noise power that is fixed to 10^{-4}.

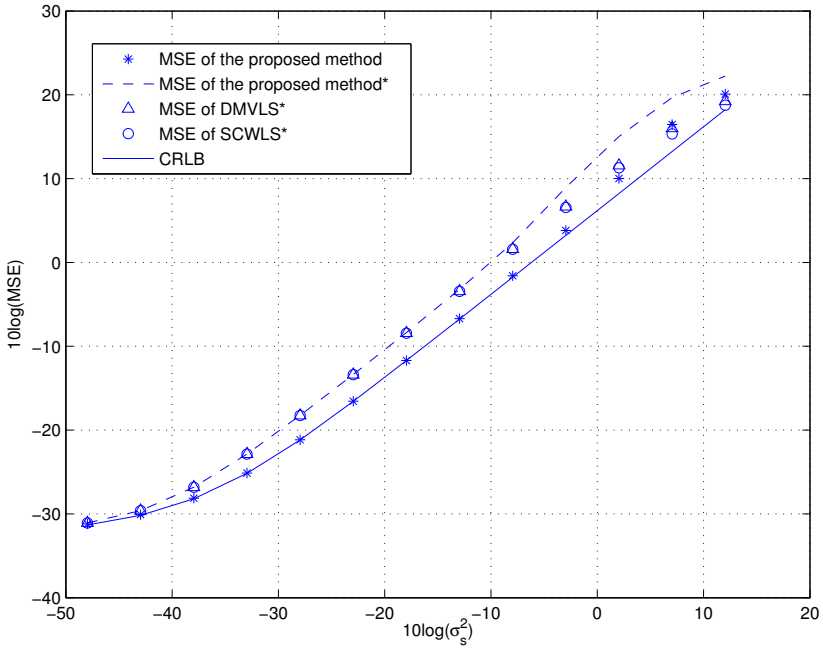

Figure 24: Performance comparison in the presence of sensor position errors with a certain 3D geometry. Star * marks the MSE when pretending sensor positions accurate.

In the Figure 24,we show the MSEs of the proposed method, DMVLS and SCWLS when pretending sensor positions accurate. When ignoring the sensor position errors, the gap between the MSEs and the CRLB becomes larger as σ_s^2 increases before σ_s^2 goes to $10^{-0.3}$. When the proposed method takes sensor position errors into account, its MSE can reach the CRLB and has the threshold effect when noise power is about $10^{-0.3}$.

4.4 Conclusion

We have expanded the new method from 2-D LER scenario to 3-D LER scenario. The theoretical analysis of the CRLB and MSE of the proposed method in the absence of sensor position errors has been stated. It is shown that the proposed estimator in 3-D is able to reach the CRLB in a wide range of TDOA measurement noise. The simulation results confirmed the theoretical development in 3-D LER scenario, and through the performance comparison with Chan-Ho, DMVLS and SCWLS, the proposed method is not only less time-consuming, but also more efficient in large TDOA measurement noise regions.

In the presence of sensor position errors under 3-D LER scenario, we took them into account in the weighting matrix and addressed the theoretical CRLB analysis. The theory has shown the proposed estimator is able to reach CRLB in the LER scenario when the sensor position errors are small. In the simulations, the performance of the proposed estimator when considering sensor position errors confirmed the theoretical development. We have also shown the performance degradation of the proposed estimator, Chan-Ho, DMVLS and SCWLS when ignoring sensor position errors.

Chapter 5

Conclusion and Future Work

We have provided an overview of source localization techniques and systems that are currently in use for various applications. Those localization techniques are usually based on four typical signal measurement models: TOA, TDOA, AOA, and RSS. After introducing those typical measurement signal models and their positioning principles, we introduced the concepts of LER based on satellite-based geolocation problems and sensor position errors.

We have presented the theoretical optimum estimation accuracy CRLB and its computation. Moreover, we introduce the nonlinear ML estimator and linear approaches LLS, including the classic Chan-Ho method and DMVLS, SCWLS for determining the source location under LER scenario. In the presence of zero-mean Gaussian measurement errors, the estimation performance of the ML and the Chan-Ho method can achieve the CRLB when the TDOA noise is small. Under the given LER scenario, Chan-Ho has a serious performance degradation while SCWLS and DMVLS can reach the CRLB.

Motivated by the practical LER localization problems, as well as the computation inefficiency and/or complex root selection strategy of SCWLS and DMVLS, we have developed this new localization algorithm. In the absence of sensor position errors, we have provided the theoretical analysis that when LER conditions are satisfied, the proposed estimator can approach the CRLB accuracy in both 2-D and 3-D. For less sufficient LER situations, iterations are applied to reduce the bias component. Different from the iterative methods such like the Taylor-series method, the proposed method does not require an initial guess. Also found by simulations with randomly distributed geometries, 5 iterations are enough to have the solutions converge and get the optimum source location estimate. Through the numerical results, it is confirmed that the proposed estimator can reach the CRLB. Compared with SCWLS and DMVLS, the proposed method is able to achieve the CRLB in a wider range of noise powers and has much shorter execution time. However, one limitation the proposed method has is that the source must be located much closer to the origin than the sensors, in another word, the source must be inside the circle bounded by the sensors, which may require some priori knowledge on source locations.

We also expand the proposed estimator to an improved version in the presence of sensor position errors. When LER is satisfied and the sensor position error is small, it's proved by the theory as well as simulations that the improved estimator can achieve the CRLB accuracy.

As a future work, the proposed estimator will be evaluated using real-world TDOA data with and without sensor position errors. Moreover, we will test the proposed method over different loose "LER" scenarios, such as GPS plus Glonass, Galileo, or wide area augmentation system (WAAS), where satellites have large but non-equal

distances to the user on Earth. More generally, one or multiple sensors may have very small sensor-source range ratios, while the other sensors satisfy the LER condition and have much larger range ratios. By studying those more general cases, we will understand the applications of the proposed estimator and its limitations better.

Bibliography

[1] O. Postolache, P. Girao, and M. Pereira, "Underwater acoustic source localization based on passive sonar and intelligent processing," in *IEEE Instrumentation and Measurement Technology Conference Proceedings, 2007. IMTC 2007.*, Warsaw, Poland, May 2007, pp. 1–4.

[2] D. Shin, S. Y. Na, J. Kim, and S. J. Baek, "Sonar localization using ubiquitous sensor network for water pollution monitoring fish robots," in *IEEE International Symposium on Signal Processing and Information Technology*, Dec 2007, pp. 80–85.

[3] D. E. Hack, L. K. Patton, B. Himed, and M. A. Saville, "On the applicability of source localization techniques to passive multistatic radar," in *2012 Conference Record of the Forty Sixth Asilomar Conference on Signals, Systems and Computers (ASILOMAR)*, Nov 2012, pp. 848–852.

[4] K. Liu, H. B. Lim, E. Frazzoli, H. Ji, and V. Lee, "Improving positioning accuracy using gps pseudorange measurements for cooperative vehicular localization," *IEEE Transactions on Vehicular Technology*, vol. 63, no. 6, pp. 2544–2556, July 2014.

[5] M. Saaid, M. Kamaludin, and M. Megat Ali, "Vehicle location finder using global position system and global system for mobile," in *2014 IEEE 5th Control and System Graduate Research Colloquium (ICSGRC)*, Aug 2014, pp. 279–284.

[6] E. Xu, Z. Ding, and S. Dasgupta, "Source localization in wireless sensor networks from signal time-of-arrival measurements," *IEEE Transactions on Signal Processing*, vol. 59, no. 6, pp. 2887–2897, June 2011.

[7] X. Li, "Performance study of rss-based location estimation techniques for wireless sensor networks," in *IEEE Military Communications Conference, 2005. MILCOM 2005.*, Oct 2005, pp. 1064–1068 Vol. 2.

[8] A. K. Chandra-Sekaran, G. Stefansson, C. Kunze, K. D. Muller-Glaser, and P. Weisser, "A range-based monte carlo patient localization during emergency response to crisis," in *Fifth Advanced International Conference on Telecommunications*, May 2009, pp. 21–26.

[9] P. R. Liu and M. Q. H. Meng, "Robotic sound source localisation algorithm with cues selection mechanism," *Electronics Letters*, vol. 44, no. 25, pp. 1493–1494, December 2008.

[10] K. C. Kwak and S. S. Kim, "Sound source localization with the aid of excitation source information in home robot environments," *IEEE Transactions on Consumer Electronics*, vol. 54, no. 2, pp. 852–856, May 2008.

[11] A. Quazi, "An overview on the time delay estimate in active and passive systems for target localization," *IEEE Transactions on Acoustics, Speech and Signal Processing*, vol. 29, no. 3, pp. 527–533, Jun 1981.

[12] M. Azaria and D. Hertz, "Time delay estimation by generalized cross correlation methods," *IEEE Transactions on Acoustics, Speech and Signal Processing*, vol. 32, no. 2, pp. 280–285, Apr 1984.

[13] R. Zekavat and R. M. Buehrer, *Handbook of Position Location: Theory, Practice and Advances*, 1st ed. Wiley-IEEE Press, 2011.

[14] F. Gustafsson and F. Gunnarsson, "Mobile positioning using wireless networks: possibilities and fundamental limitations based on available wireless network measurements," *IEEE Signal Processing Magazine*, vol. 22, no. 4, pp. 41–53, July 2005.

[15] D. N. Hatfield, "A report on technical and operational issues impacting the provision of wireless enhanced 911 services," *Federal Communication Commission, Tech. Rep*, 2002.

[16] B. T. Fang, "Simple solutions for hyperbolic and related position fixes," *IEEE Transactions on Aerospace and Electronic Systems*, vol. 26, no. 5, pp. 748–753, Sep 1990.

[17] J. O. Smith and J. S. Abel, "The spherical interpolation method of source localization," *IEEE Journal of Oceanic Engineering*, vol. 12, no. 1, pp. 246–252, Jan 1987.

[18] Y. T. Chan and K. C. Ho, "A simple and efficient estimator for hyperbolic location," *IEEE Transactions on Signal Processing*, vol. 42, no. 8, pp. 1905–1915, Aug 1994.

[19] N. Patwari, J. N. Ash, S. Kyperountas, A. O. Hero, R. L. Moses, and N. S. Correal, "Locating the nodes: cooperative localization in wireless sensor networks," *IEEE Signal Processing Magazine*, vol. 22, no. 4, pp. 54–69, July 2005.

[20] D. Niculescu and B. Nath, "Ad hoc positioning system (aps) using aoa," in *INFOCOM 2003. Twenty-Second Annual Joint Conference of the IEEE Computer and Communications. IEEE Societies*, vol. 3, March 2003, pp. 1734–1743 vol.3.

[21] A. Dubrovin, V. Nikishov, and T. Shevgunov, "Combined aoa/tdoa passive radar for airport landing system," in *2014 Tyrrhenian International Workshop on Digital Communications - Enhanced Surveillance of Aircraft and Vehicles (TIWDC/ESAV)*, Sept 2014, pp. 72–77.

[22] H. L. Song, "Automatic vehicle location in cellular communications systems," *IEEE Transactions on Vehicular Technology*, vol. 43, no. 4, pp. 902–908, Nov 1994.

[23] T. Eren, W. Whiteley, and P. Belhumeur, "Using angle of arrival (bearing) information in network localization," in *2006 45th IEEE Conference on Decision and Control*, Dec 2006, pp. 4676–4681.

[24] H. C. Chen, T. H. Lin, H. T. Kung, C. K. Lin, and Y. Gwon, "Determining rf angle of arrival using cots antenna arrays: A field evaluation," in *2012 - MILCOM 2012 MILITARY COMMUNICATIONS CONFERENCE*, Oct 2012, pp. 1–6.

[25] A. J. Weiss, "On the accuracy of a cellular location system based on rss measurements," *IEEE Transactions on Vehicular Technology*, vol. 52, no. 6, pp. 1508–1518, Nov 2003.

[26] D. Qiao and G. K. H. Pang, "An iteratively reweighted least square algorithm for rss-based sensor network localization," in *2011 International Conference on Mechatronics and Automation (ICMA)*, Aug 2011, pp. 1085–1092.

[27] A. Koneru, X. Li, and M. Varanasi, "Comparative study of rss-based collaborative localization methods in sensor networks," in *IEEE Region 5 Conference*, April 2006, pp. 243–248.

[28] B. J. Dil and P. J. M. Havinga, "On the calibration and performance of rss-based localization methods," in *Internet of Things (IOT), 2010*, Nov 2010, pp. 1–8.

[29] S. Bancroft, "An algebraic solution of the gps equations," *IEEE Transactions on Aerospace and Electronic Systems*, vol. AES-21, no. 1, pp. 56–59, Jan 1985.

[30] W. H. Foy, "Position-location solutions by taylor-series estimation," *IEEE Transactions on Aerospace and Electronic Systems*, vol. AES-12, no. 2, pp. 187–194, March 1976.

[31] P. Misra and P. Enge, *Global positioning system: signals, measurements, and performance*. Ganga-Jamuna Press, 2006. [Online]. Available: http://books.google.com/books?id=pv5MAQAAIAAJ

[32] E. Choi and D. A. Cicci, "Analysis of gps static positioning problems," *Applied Mathematics and Computation*, vol. 140, no. 1, pp. 37 – 51, 2003. [Online]. Available: http://www.sciencedirect.com/science/article/pii/S0096300302001935

[33] L. A. Romero, J. Mason, and D. M. Day, "The large equal radius conditions and time of arrival geolocation algorithms," *SIAM Journal on Scientific Computing*, vol. 31, no. 1, pp. 254–272, 2008.

[34] L. Lin, H. So, F. K. Chan, Y. Chan, and K. Ho, "A new constrained weighted least squares algorithm for tdoa-based localization," *Signal Processing*, vol. 93, no. 11, pp. 2872 – 2878, 2013. [Online]. Available: http://www.sciencedirect.com/science/article/pii/S016516841300145X

[35] Z. Ma and K. C. Ho, "Toa localization in the presence of random sensor position errors," in *2011 IEEE International Conference on Acoustics, Speech and Signal Processing (ICASSP)*, May 2011, pp. 2468–2471.

[36] K. C. Ho, X. Lu, and L. Kovavisaruch, "Source localization using tdoa and fdoa measurements in the presence of receiver location errors: Analysis and solution," *IEEE Transactions on Signal Processing*, vol. 55, no. 2, pp. 684–696, Feb 2007.

[37] K. C. Ho and L. Yang, "On the use of a calibration emitter for source localization in the presence of sensor position uncertainty," *IEEE Transactions on Signal Processing*, vol. 56, no. 12, pp. 5758–5772, Dec 2008.

[38] S. Srirangarajan, A. Tewfik, and Z. Q. Luo, "Distributed sensor network localization with inaccurate anchor positions and noisy distance information," in *IEEE International Conference on Acoustics, Speech and Signal Processing, 2007. ICASSP 2007.*, vol. 3, April 2007, pp. III–521–III–524.

[39] S. MartíNez and F. Bullo, "Optimal sensor placement and motion coordination for target tracking," *Automatica*, vol. 42, no. 4, pp. 661–668, 2006.

[40] K. B. Purvis, K. J. Astrom, and M. Khammash, "Estimation and optimal configurations for localization using cooperative uavs," *IEEE Transactions on Control Systems Technology*, vol. 16, no. 5, pp. 947–958, Sept 2008.

[41] A. Griffin, D. Pavlidi, M. Puigt, and A. Mouchtaris, "Real-time multiple speaker doa estimation in a circular microphone array based on matching pursuit," in *2012 Proceedings of the 20th European Signal Processing Conference (EUSIPCO)*, Aug 2012, pp. 2303–2307.

[42] S. Richter and L. Fusillo, "Helicopter navigation algorithms for the placement of sonobuoys in an antisubmarine warfare (asw) environment," in *Proceedings of the IEEE 1988 National Aerospace and Electronics Conference, 1988. NAECON 1988.*, May 1988, pp. 280–286 vol.1.

[43] S. M. Kay, *Fundamentals of Statistical Signal Processing: Estimation theory*, ser. Fundamentals of Statistical Signal Processing. Prentice Hall, Inc., 1993. [Online]. Available: http://books.google.com/books?id=aFwESQAACAAJ

[44] K. W. Cheung, H. C. So, W. K. Ma, and Y. T. Chan, "A constrained least squares approach to mobile positioning: algorithms and optimality," *EURASIP journal on applied signal processing*, vol. 2006, pp. 150–150, 2006.

[45] L. A. Romero and J. Mason, "Evaluation of direct and iterative methods for overdetermined systems of toa geolocation equations," *IEEE Transactions on Aerospace and Electronic Systems*, vol. 47, no. 2, pp. 1213–1229, April 2011.

[46] M. A. Woodbury, "Inverting modified matrices," *Memorandum report*, vol. 42, p. 106, 1950.